Journal of Constructional Steel Research 212 (2024) 108314

Contents lists available at ScienceDirect

Journal of Constructional Steel Research

journal homepage: www.elsevier.com/locate/jcsr

Non-linear component-based modelling strategy for beam-to-column steel-concrete composite joints under seismic loads

Marco Fasan [a], Chiara Bedon [a,*], Claudio Amadio [a], Maria Rosaria Pecce [b]

[a] University of Trieste, Department of Engineering and Architecture, Italy
[b] University of Napoli Federico II, Department of Structures for Engineering and Architecture, Italy

ARTICLE INFO

Keywords:
Steel-concrete composite joints
Seismic loading
Component-based modelling
Cyclic non-linear behaviour
Resistance
Stiffness

ABSTRACT

This paper proposes and validates a computationally efficient, non-linear numerical macro-modelling strategy to predict and assess the global and local response of steel-concrete composite joints, when subjected to seismic loads. The reference numerical model takes the form of a component-based strategy in which each component can be efficiently characterized in resistance and stiffness terms, and each constituent material has a typical non-linear behaviour with hysteresis (Takeda model for concrete, Pivot model the T-stub components and kinematic model for all the other steel members). The major advantage is the possibility to adapt the same unified modelling strategy to different configurations of steel-concrete composite joints, which may differ for geometrical and mechanical configurations of constituent members, position of joint (i.e., interior or exterior), connection type (welded or bolted), etc. As shown, due to the presented modelling approach, even under simplified assumptions, a rather close agreement is generally found between the present numerical predictions and the cyclic response of a selection of three different steel-concrete composite joints of literature, which have been investigated on full-scale experimental configurations. Most importantly, the contribution of steel members and the concrete slab can be efficiently taken into account, and allow to develop the typical mechanisms in which the slab itself is involved for the complex performance of composite frames under seismic events.

1. Introduction

The design of seismic resistant steel-concrete composite joints and frames is a challenging task and is mostly affected by a multitude of geometrical and mechanical parameters, which typically manifest in different stiffness and resistance properties of components, and thus in different possible mechanisms and load bearing capacities for the assembled joints and frame systems [1–3].

While for steel or concrete structures, individual design (and modelling) strategies for their mechanical optimization under seismic loads have been explored and addressed in the years by many research studies, see for example, [4–6], further efforts for steel-concrete composite systems – in which even more complex mechanical interactions take place – are still needed.

The existing provisions of EC3 [7] and EC4 [8], more in detail, are useful for the design, verification and mechanical modelling of joints which are mostly affected by negative bending moments only, as in the case of ordinary vertical loads only on the frame object of study. Under seismic loading, it is well known that the design bending moment acting in the composite joint can be also positive, which involves compression in the concrete slab. While the steel members can be still designed and mechanically characterized as recommended in EC3, for the concrete slab it is required to follow the EC4 and EC8 recommendations ([9] Annex C), which are specifically elaborated for concrete in tension or compression, and are based on literature experimental evidences from [10,11]. The basic assumption of these recommendations is that the steel-concrete composite beams have a typical "T" section, the connection of beam and slab is fully rigid and plastic hinges due to design bending moments take place in the beam only, rather than in the beam-to-column joint. In order to ensure appropriate resistance and stiffness, but also a mostly ductile failure mechanism to a general steel-concrete composite joint, specific design rules need thus to be taken into account, as also recommended in the Italian technical document for the design of steel-concrete composite frame under seismic loading, which was elaborated in the framework of the DPC-ReLUIS Italian project [12].

For real structural systems under seismic loading, moreover, it is well known that the mechanical response is rather complex and uncertain to describe, and often affected by a multitude of parameters, such as the

* Corresponding author at: Via Valerio 6/1, 34127 Trieste, Italy.
E-mail address: chiara.bedon@dia.units.it (C. Bedon).

https://doi.org/10.1016/j.jcsr.2023.108314
Received 11 September 2023; Received in revised form 27 October 2023; Accepted 30 October 2023
Available online 3 November 2023

geometrical and mechanical properties of components (Section 2). This is especially the case of steel-concrete composite joints, where several types and configurations of members (i.e., Fig. 1), their detailing, the joint positions in a given frame (i.e., exterior or interior joint), as well as the applied bending moment are typical major influencing parameters for structural considerations. In this sense, full-scale experimental analyses [13–15] or computationally expensive and modelling approach are often required [16–18].

In this paper, the attention goes especially to the refinement and assessment of a computationally efficient, simplified component-based modelling approach, which is proposed as harmonized procedure in support of design for a multitude of configurations of steel-concrete composite joints like in Fig. 1, when subjected to seismic loading. Differing from extremely complex and time expensive 3D Finite Element numerical models (see for example Fig. 2 (a) and [17]), the potential of cost-minimized component-based strategies like in Fig. 2 (b) is assessed for cyclic assessment purposes.

Most importantly, compared to simplest rigid-plastic component-based procedures like in [9], or previous simplified literature applications like in [19–24], non-linear axial springs are efficiently used to mechanically describe the active joint components under seismic loads, and to account for the occurrence of multiple and complex mechanisms in cyclic conditions. In doing so, a major advantage is taken from the combination of existing background provisions (i.e., [7–9,12]), but also by the definition of additional specific contributions that need to be considered for the resistance parameters and stiffness coefficients representative of the superimposed concrete slab, and its interaction with the steel members of the frame object of study (Section 3). The final numerical methodology represents, as a whole, the exploitation of previous efforts undertaken in [19,20,22]. Differing from past applications, as shown, the non-linear performance assessment of joints under seismic loading is realistically reproduced thanks to a major contribution of the slab interaction with the metal frame, which includes also the steel rebars which are responsible of the structural continuity in the region of column.

To this aim, the slab contributions in tension and compression are thus shortly exploited in Section 3. To support the design considerations of Section 3, three different practical numerical examples are presented in Section 4, where monotonic and cyclic numerical responses are addressed towards literature experiments. As shown, based on the selection of validation experiments, the non-linear cyclic performance of differently arranged and even complex steel-concrete composite joints (both bolted and welded, interior and exterior) can be properly taken into account, and the involved resisting mechanisms can be efficiently described by means of the proposed computationally efficient numerical procedure. In this regard, the present numerical application further confirms the potential of the design methodology elaborated in [12], as well as proves the progressive optimization of past numerical efforts from [19,20,22], as also confirmed by the selected experimental comparisons. As a fact, the component-based strategy still preserves some intrinsic limits (such as the lack of detailed component analysis and damage evolution in the concrete slab), but represents a practical tool of unified efficiency. Also, the presented comparisons suggest its suitability and efficiency for the seismic analysis of full steel-concrete composite joints, which will be further addressed and investigated in next research developments.

2. Component-based modelling strategy for steel-concrete composite joints

2.1. General considerations

Assured that the key step of component-based modelling is represented by the definition of the moment-rotation constitutive law of the assembled joint (see Fig. 3 (a)), a major challenge is represented by the detection of all the active components in steel or concrete members. In this regard, it is worth to remind that steel-concrete composite joints often lack of symmetry. This could require, especially under seismic loading, major efforts for the mechanical characterization of all possible phenomena, see Fig. 3 (b).

For the design of steel structures and joints subjected to seismic loading, rules for component-based modelling approaches are usually based on the EC3 provisions. EC4 rules, where possible, can be adapted for the concrete slab. Presently, however, the major weakness of existing standards like EC3 and EC4 is that component-based rules are mostly defined for steel and steel-concrete joints under negative bending moment, i.e., for frames under vertical loads only. The seismic loading condition, which necessarily involves a change in the design bending

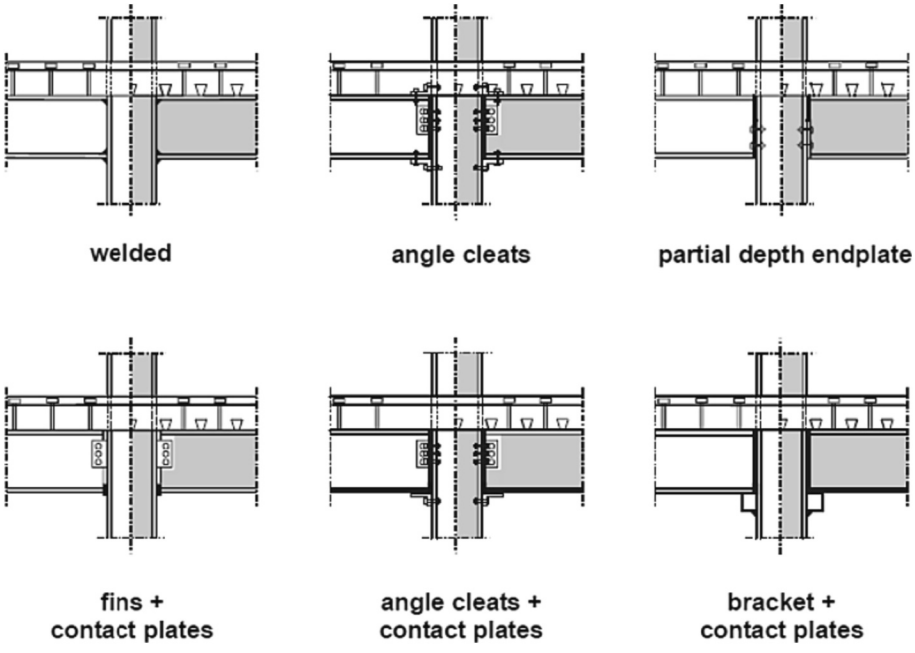

Fig. 1. Examples of possible configurations of steel-concrete composite joints (EC4).

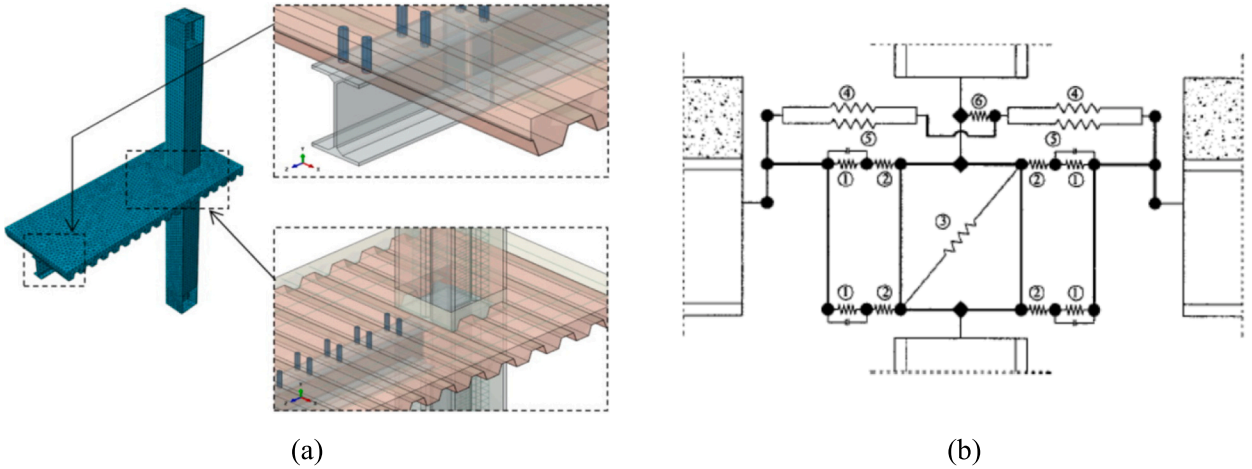

Fig. 2. Examples of modelling strategies for steel-concrete composite joints: (a) refined full 3D Finite Element numerical model (reproduced from [17] with permission from Elsevier©, copyright license number 5619240622715, August 2023); (b) preliminary component-based numerical model (adapted from [22]).

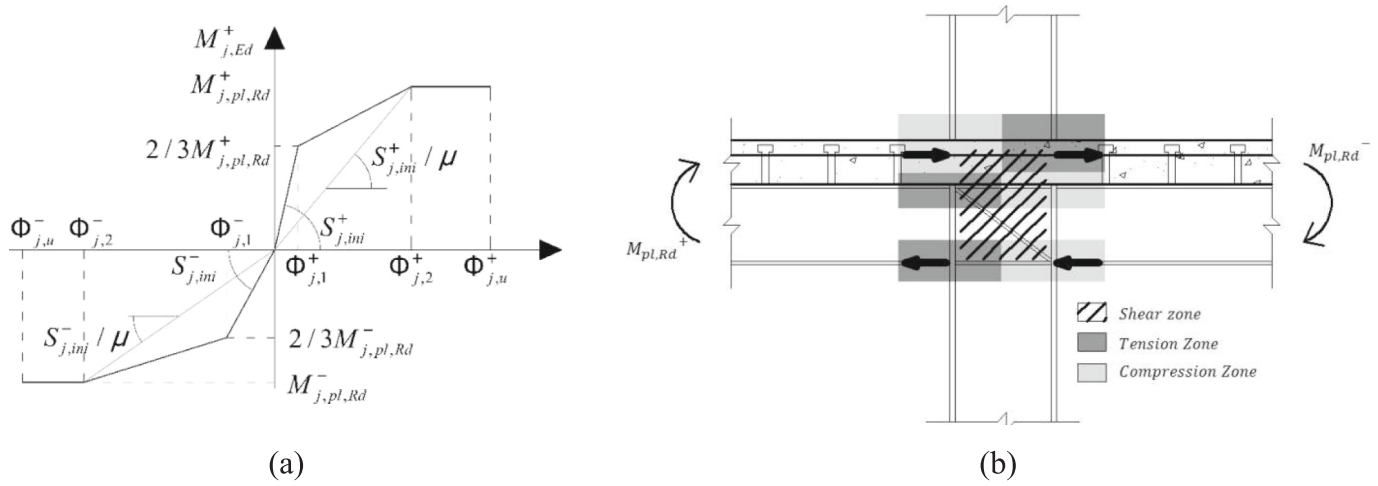

Fig. 3. Mechanical characterization of composite joints: (a) typical multi-linear moment-rotation constitutive law and (b) detection of active components in a steel-concrete composite joint under seismic loading.

moment, is still not properly addressed.

When the concrete slab with its rebars and stirrups is also taken into account to mechanically interact with the steel frame members, the major complexity derives, in a simplified modelling point of view, from the need of characterizing a number of additional mechanical phenomena in which the slab itself can interact with steel members of the frame, and thus their mechanical features are mutually affected. As known, these phenomena are different for the slab in tension and compression, and for seismic loading conditions – in which the bending moment sign changes – this represents a key step of design.

To summarize, while it is in fact expected that the slab contribution is mostly affected by:

- Longitudinal rebars in tension, for the steel-concrete composite joint under hogging bending moment (i.e., downward deflection), and
- Concrete crushing, when the joint is subjected to sagging bending moment (i.e., upward deflection).

Many other behaviours should be efficiently taken into account, as it is for example for welded or bolted steel-concrete composite joints involving a multitude of components and geometrical / mechanical variables.

To overcome these uncertainties and modelling difficulties, this paper elaborates on a unified component-based characterization of efficient numerical procedures, and validates the proposal discussed in [12]. A major attention is spent for the identification and resistance / stiffness characterization of possible mechanisms in the concrete slab, which are shortly recalled in Section 3.

2.2. Resistance

For a composite joint like in Fig. 3, the resisting bending moment depends on the effective resistance of each active component $F_{r,Rd}$, multiplied by the distance of each component h_r from a reference control point of the joint:

$$M_{j,pl,Rd} = \sum_{i=1}^{r} F_{r,Rd} h_r \tag{1}$$

Depending on the composite joint features, the number of components to include in Eq. (1) may largely change. As far as the category of steel members with welded or bolted joints are taken into account respectively, basic component modelling rules as in EC3 can be used for metal components. These are summarized in Tables 1 and 2. To note that the contribution of the concrete slab, both in tensile or compressive region for the active components (depending on the applied bending moment), is considered in in Tables 1-2 and further discussed, for the

Table 1
Component characterization for a welded steel-concrete composite joint.

Joint zone	Component
Tension	Column flange in bending [§EC3 1–8 6.2.6.4.3] Column web in tension [§EC3 1–8 6.2.6.3] Longitudinal rebars for the slab in tension [Section 3]
Compression	Column flange in bending [§EC3 1–8 6.2.6.4.3] Column web in compression [§EC3 1–8 6.2.6.2] Slab in compression [Section 3]
Shear	Column web panel in shear [§EC3 6.2.6.1]

Table 2
Component characterization for a bolted steel-concrete composite joint.

Joint zone	Component
Tension	Longitudinal rebars for the slab in tension [Section 3] Bolt in tension [§EC3 1–8, 3.4] Punching [§EC3 1–8, 3.4] Column web in tension [§EC3 1–8 6.2.6.3] Column flange in bending [§EC3 1–8 6.2.6.4.1–2] Flange in bending [§EC3 1–8 6.2.6.5] Beam web in tension [§EC3 1–8 6.2.6.8]
Compression	Column flange in bending [§EC3 1–8 6.2.6.4.3] Column web in compression [§EC3 1–8 6.2.6.2] Slab in compression [Section 3]]
Shear	Column web panel in shear [§EC3 6.2.6.1]

present proposal, in accordance with Section 3.The most important aspect in these tables is that the concrete slab with its rebars can show the well-known mechanisms (1 to 3) which guide the design and optimization of joint components themselves [12]. As far as the concrete slab is not in direct contact with the frame column [18], moreover, the additional mechanism 4 may take place, and need to be properly considered and quantified [12], or even strengthened [25].

2.3. Stiffness

Similar to resistance considerations, depending on the design bending moment on the active components which belong to the steel-concrete composite joint object of study, stiffness coefficients also necessitate a specific mechanical analysis and characterization. Steel stiffness contributions are listed in Tables 1-2 and can be rationally expressed as for EC3 provisions, where it is assumed that multiple axial springs are used to represent each member (i.e., column web, bolts, flange, etc.), see Fig. 4.

In accordance with the typical relationship schematized in Fig. 3 (a), the global initial stiffness of the joint is in fact well described as (up to $2/3M_{j,pl,Rd}$):

$$S_{j,ini} = -d_{CR}\sum_{r=1}^{n} k_{eff,r}h_r + \sum_{r=1}^{n} k_{eff,r}h_r^2 \tag{2}$$

where:

$$k_{eff,r} = \frac{1}{\sum 1/k_{i,r}} \tag{3}$$

and:

$$d_{CR} = \frac{\sum_{r=1}^{n} k_{eff,r}h_r}{\sum_{r=1}^{n} k_{eff,r}} \tag{4}$$

The secant stiffness term as in Fig. 3 (a) is then given by $S_{j,ini}/\mu$, where:

$$\mu = \left(1.5\frac{M_{j,Ed}}{M_{j,pl,Rd}}\right)^{\psi} \tag{5}$$

with:

$$\varphi_{j,1} = 2/3M_{j,pl,Rd}/S_{j,ini} \tag{6}$$

$$\varphi_{j,2} = \left(M_{j,pl,Rd}\right)/\left(S_{j,ini}/\mu\right) \tag{7}$$

As for resistance characterization, the presence of a superimposed concrete slab which interacts with the steel frame members should be properly taken into account for an efficient mechanical modelling of joint. To this aim, basic rules are summarized in Section 3.

3. Mechanical characterization of slab contributions

3.1. Concrete slab in compression

3.1.1. Resistance

The compressed slab can offer a maximum design resistance $F_{c,slab,Rd}$ which strictly depends on the geometrical configuration of the joint, and thus on the possible mechanisms that the slab itself can undertake under external bending moment. For an exterior composite joint with $i = 3$ possible mechanisms of the slab in contact, see [12,26] it is assumed that:

$$F_{c,slab,Rd} = \sum F_{Rd,i} \tag{8}$$

For an interior joint like in Fig. 5 and under seismic loading, conversely, the compressive capacity of the slab is given by:

$$F_{c,slab,Rd} = \sum F_{Rd,i} - A_s f_{yd,l} \tag{9}$$

The possible mechanisms 1, 2 and 3 required in Eqs. (8)–(9) for the characterization of concrete in compression are schematized in Fig. 6. To summarize, it is assumed that for mechanism 1, which is associated to the direct compression of the concrete strut on the column, the resistance term is given by (Fig. 6 (a)):

$$F_{Rd,1} = b_b d_{eff}(0.85f_{ck}/\gamma_c) \tag{10}$$

where $b_b$represents the width of contact section (i.e., the column flange), $d_{eff}$is the effective height of the slab (corresponding to its total thickness,

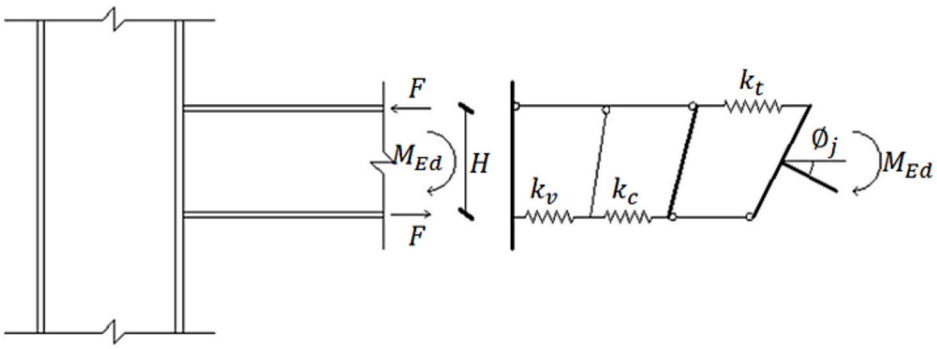

Fig. 4. Component-based mechanical model for a steel joint under negative bending moment (example).

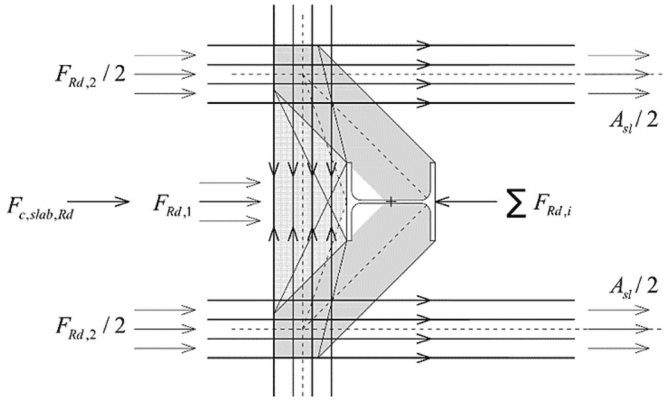

Fig. 5. Typical resisting mechanism for an interior joint.

for solid section), while f_{ck} and γ_c are the characteristic strength in compression and the partial safety factor for concrete. To note that this type of mechanism is usually activated for the slab in compression (positive bending moment) but can also take place in the slab under negative bending moment. For mechanism 2, which is associated to the spread of two compressed struts on the web of column, it is assumed that (Fig. 6 (b)):

$$F_{Rd,2} = 0.7 h_c d_{eff} (0.85 f_{ck}/\gamma_c) \tag{11}$$

with h_c the column height. For mechanism 3, which can offer a resistance proportional to the number and size of small struts in compression against the n shear studs, it is finally (Fig. 6 (c)):

$$F_{Rd,3} = nP_{Rd} \tag{12}$$

where:

$$P_{Rd} = min\left(\frac{0.8 f_u \pi d_{sc}^2/4}{\gamma_v};\ \frac{0.29 \alpha d_{sc}^2 \sqrt{f_{ck} E_{cm}}}{\gamma_v}\right) \tag{13}$$

represents the design strength of a single shear stud with diameter d_{sc}, ultimate strength f_u and length h_{sc}. To note that $\alpha = 1$ when $h_{sc}/d_{sc} > 4$ and $\alpha = 0.2(h_{sc}/d_{sc} + 1)$ when $3 < h_{sc}/d_{sc} < 4$, while $\gamma_v = 1.25$ is the partial safety factor.

3.1.2. Stiffness

The stiffness characterization of a concrete slab belonging to a composite joint actually represents a major uncertainty, and the existing design standards do not provide specific recommendations. In this regard, based on previous studies reported in [12,26], it is assumed that the stiffness coefficient is given by:

$$k_c = k_{c,1} + k_{c,2} \tag{13}$$

where k_c depends on the contributions of mechanisms 1 and 2 acting in parallel for the compressed slab, which can be separately calculated in accordance with [12,22,27], see Fig. 7. In doing so, the calculation approach is based on the homogenisation of the concrete section to steel components.

More in detail, for mechanism 1, it is assumed that:

$$k_{c,1} = \frac{A_c E_{cm}}{h_c E_s} = \frac{(b_b h_c) E_{cm}}{h_c E_s} \tag{15}$$

Eq. (15) accounts for the stiffness contribution which derives from the compressed strut on the column web, with total length h_c (see Fig. 7 (a)), where E_{cm} and E_s represent the elastic modulus of concrete and steel respectively. The stiffness coefficient for mechanism 2 (Fig. 7 (b)) is still associated to the strut-and-tie response of the slab, and can be quantified as:

$$k_{c,2} = \frac{2}{\frac{1}{k_s\left(1+\left(\frac{l_y}{l_x}\right)^2\right)} + \frac{1}{k_t\left(\frac{l_y}{l_x}\right)^2}} = \frac{2}{\frac{1}{2k_s} + \frac{1}{k_t}} \tag{16}$$

For a single strut (s) and tie (t), the contribution in stiffnes terms is given by:

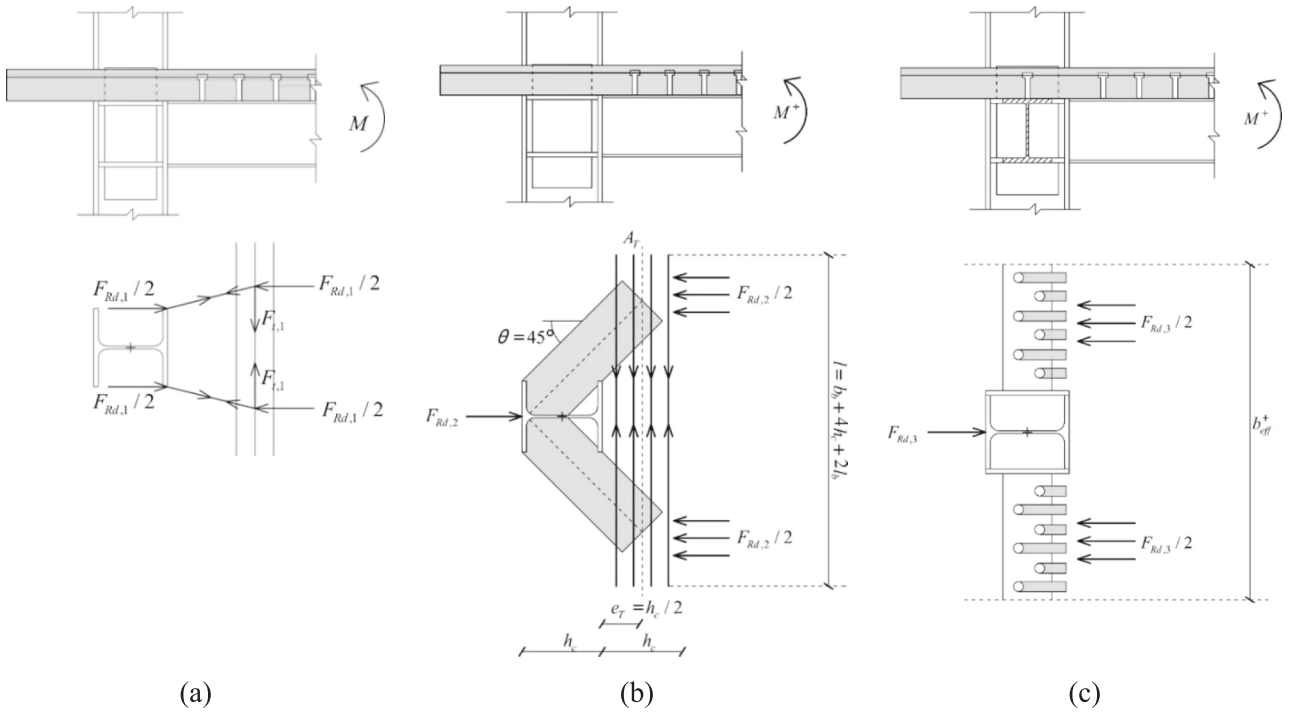

Fig. 6. Reference mechanisms for the concrete slab in compression: (a) mechanism 1; (b) mechanism 2; (c) mechanism 3.

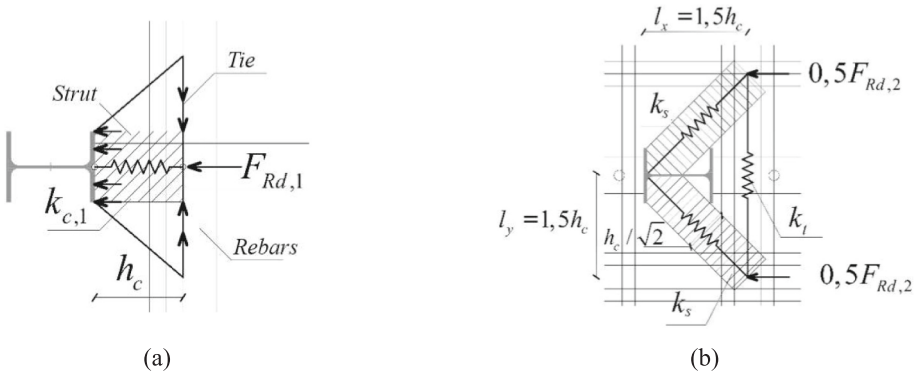

Fig. 7. Stiffness coefficients for the slab in compression: contributions of (a) mechanism 1 and (b) mechanism 2.

$$k_s = \frac{A_s}{\sqrt{l_x^2 + l_y^2}} \frac{E_{cm}}{E_s} = \frac{0.7 h_c d_{eff}}{\sqrt{1.5h_c^2 + 1.5h_c^2}} \frac{E_{cm}}{E_s} \tag{17}$$

$$k_t = \frac{A_T}{l_y} = \frac{A_T}{1.5h_c} \tag{18}$$

with A_s, A_t their cross-sectional area respectively, and A_T the cross-section of transversal rebars.

3.2. Concrete slab in tension

3.2.1. Resistance

As previously discussed, the resistance in tension is mostly governed by the longitudinal rebars, and their contribution (with total cross-section A_{sl}) can be quantified as:

$$F_{t,slab,Rd} = A_{sl}\left(f_{yk,l}/\gamma_s\right) = A_{sl} f_{yd,l} \tag{19}$$

Under this assumption, however, it is important to remind that all the mechanisms 1, 2 and 3 of concrete can take place, as schematized in Fig. 8. While the resistance contribution for each mechanism is still given by Eqs. (10), (11) and (12) respectively, the joint should be properly designed to ensure a ductile failure mechanism.

For mechanism 1 (Fig. 8 (a)), this behaviour can be achieved as far as the total area of longitudinal rebars is limited to:

$$A_{s,1} \le \frac{F_{Rd,1}}{f_{yd,l}} = b_c d_{eff} \left(\frac{0.85 f_{ck}/\gamma_c}{f_{yk,l}/\gamma_s} \right) \tag{20}$$

For mechanism 2 (Fig. 8 (b)), the cross-sectional area of longitudinal steel rebars should not exceed:

$$A_{s,2} \le \frac{F_{Rd,2}}{f_{yd,l}} = 0.7 h_c d_{eff} \left(\frac{0.85 f_{ck}/\gamma_c}{f_{yk,l}/\gamma_s} \right) \tag{21}$$

Finally, for mechanism 3 in Fig. 8 (c), it is recommended that:

$$A_{s,3} \le \frac{F_{Rd,3}}{f_{yd,l}} \tag{22}$$

Additional remarks should be also taken into account for the optimal design of transversal rebars, see [12].

3.2.2. Stiffness

In terms of stiffness characterization of the slab in tension, the major contribution is certainly associated to the longitudinal rebars. In accordance with EC4 [8], it is in fact assumed that:

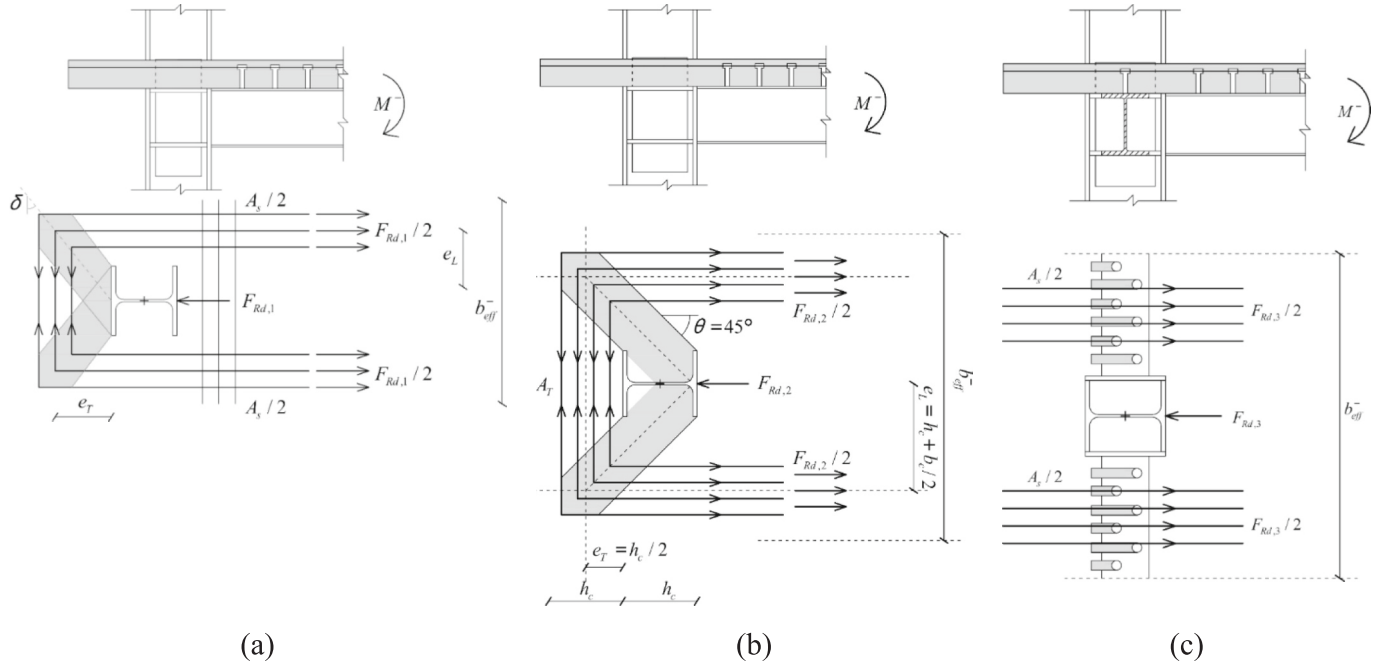

Fig. 8. Reference mechanisms for the concrete slab in tension: (a) mechanism 1; (b) mechanism 2; (c) mechanism 3.

$$k_{s,r,slip} = \frac{A_{sl}}{l_r} k_{slip} \tag{23}$$

where k_{slip} accounts for the shear deformation of the slab [28] and l_r is the effective length of rebars [29]. For exterior or interior joints, this term is respectively equal to:

$$l_r = \frac{h_c}{2} + 0.8z \tag{24}$$

$$l_r = 2(h_c + z) \tag{25}$$

with z the distance of middle axis of rebar and bottom beam flange.

4. Assessment of the component-based modelling strategy

4.1. General numerical approach

The present modelling strategy is based on the use of a commercial computer software (in this case, Sap2000 software [30]) in which simple tools and mechanical models are used to describe the non-linear performance of each joint component and constituent material. In doing so, in particular, the modelling approach assumes that a given composite frame configuration can be efficiently described as follows:

a) Non-linear links ("NL-link type" from Sap2000 library) are used to account for the geometric response of each joint component, based on a "multilinear plastic" characterization and input description which is based on the Equations summarized in Sections 2–3;
b) Weightless "Rigid Link" elements are considered to connect the NL-links;
c) Non-linear stress-strain relationships are taken into account for steel and concrete materials, and concrete is considered to react only in compression. When possible (as in the presently discussed examples), experimental material properties and stress-strain relationships should be privileged. An example of present validation is proposed in Fig. 9;
d) Frame elements with uniform, equivalent inertial properties are used for the steel-concrete composite beams in the analysis of the examined frames ("section designer" tool). In particular, separate elements are used to describe the steel beam (i.e., web and flanges), in order to account for specific mechanical properties (see point (c)). Also, steel rebars are geometrically described by nominal section properties and placed in their actual position in the slab;
e) Regarding the hysteretic behaviour of each joint material and component under cyclic loading, a Takeda model is used for concrete elements, a Pivot model is considered for the T-stub components and a kinematic model is used for all the other steel members.

Finally, for the comparative analysis of numerical results with selected experimental evidences from literature, it is important to remind that mean values are considered for the mechanical properties of steel and concrete, in place of characteristic values. Accordingly, the partial safety factors for the Equations described in Sections 2–3 are also set equal to 1.

4.2. Model #1 – Exterior welded joint

The first examined specimen is the exterior steel-concrete composite joints which was also experimentally and numerically investigated in [17]. The welded joint sample, see Fig. 10, was characterized by a 330 mm long concrete cantilever edge strip (from the exterior flange of the column) and an IPE240 steel beam, which was directly welded to a 3400 mm long partially encased, HE280B composite column section. The concrete slab was connected to the steel beam profile by means of studs as in Fig. 10. The experimental setup included a cyclic loading protocol with a vertical force at the free end of the cantilever arm, see Fig. 10 (d). To note in Fig. 10 (a) that the web panel of the column was characterized by the presence of a 10 mm thick stiffener plate. The experimental performance of the specimen was discussed in [17], with the support of a refined full 3D numerical model developed in Abaqus [31], see Fig. 2 (a), which is shortly recalled herein for further assessment of the present component-based modelling approach.

For the present analysis, the composite joint is schematized in terms of components like in Fig. 11.

More in detail, the set of non-linear links (axial springs) is used to mechanically describe:

- #1: the column web panel in shear (below the stiffener steel plate);
- #2: the column web panel in shear (above the stiffener);
- #3 and #4: the column web panel under compression or tension, due to the force which is transferred from the top and bottom beam flanges to the column;
- #5a and #5b ("l" left and "r" right): mechanisms 1 and 2 for the concrete slab. To note that both these springs are placed on the barycentric axis of the slab;
- #6: longitudinal rebars in tension.

Basic steel components can be mechanically characterized in accordance with EC3 [7], see Annex I.

To summarize, a symmetric elastic-plastic behaviour in tension and

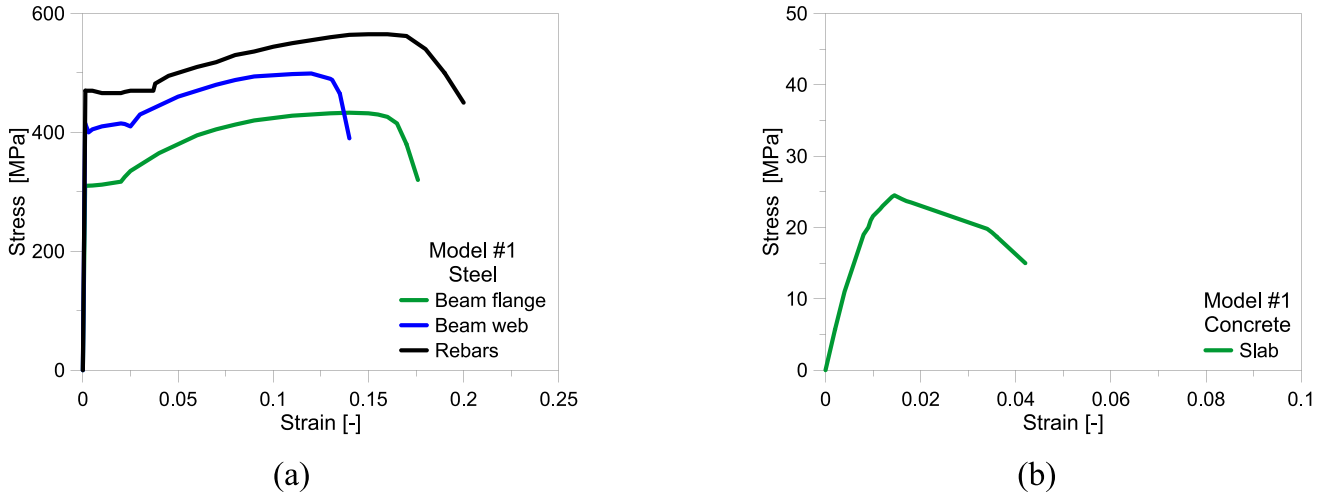

Fig. 9. Example of input stress-strain relationships for (a) steel and (b) concrete materials.

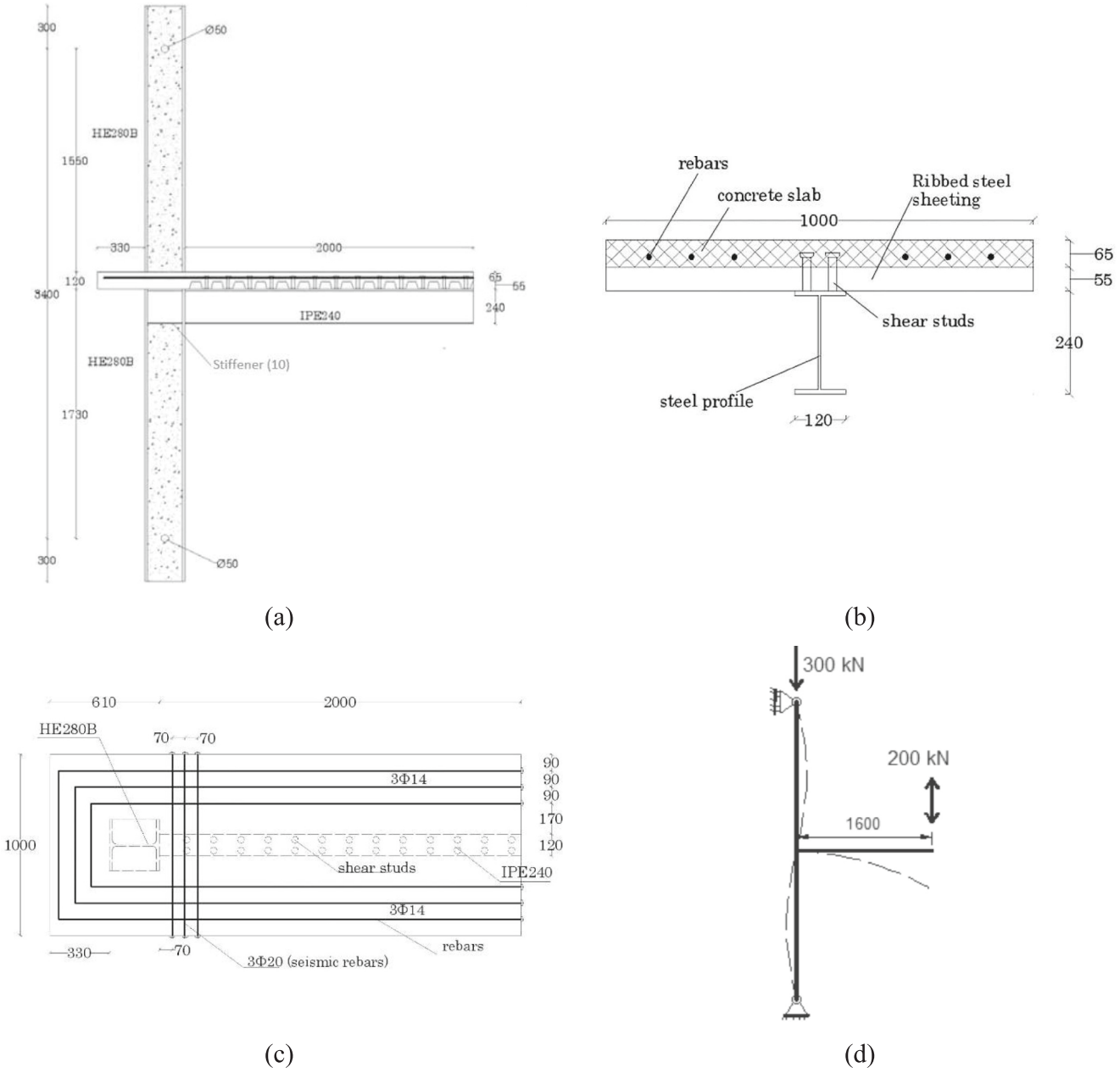

Fig. 10. Reference exterior welded joint: (a) side view; (b) cross-section; (c) top view and (d) experimental setup (dimensions in mm).

compression is assigned to component #1 and component #2, with kinematic performance under cyclic loading. The hardening brunch after yielding is set with 1% slope. For the column web under transverse tension or compression (components #3 and #4) the constitutive law is necessarily unsymmetrical, with elastic-plastic hardening in compression (inactive link in tension). As for components #1 and #2, the 1% slope is taken into account for hardening after yielding.

To note that the links #5ar, #5al and #5bl, #5br are used to take into account the resistance terms and stiffness coefficients of the concrete slab, on both the sides of the column / joint.

In this regard, for mechanism 1 it is assumed that the resistance of the slab is given by Eq. (10), with $b_b = 280$ mm, $d_{eff} = 65$ mm, $f_{c,k} = 24.8$ MPa, and thus resulting in $F_{Rd,1} = 376$ kN (with $\gamma_c = 1$). The stiffness coefficient, based on Eq. (15), results equal to 41.7 mm.

The force-elongation constitutive law of link #5a representing the mechanism 1 of the concrete slab is thus assembled considering that (see Fig. 12 (a)):

- concrete reacts only in compression;
- $\delta_y = F_{rd,1}/E_{cm}k_{c,1}$ = -0.288 mm represent the yielding deformation for crushing;
- $\delta_u = -1.12$ mm represents the ultimate elongation of concrete slab in compression (which is associated to a maximum strain of 4‰ for the compressed concrete strut). To note that the maximum strain exceeds the usual 3.5‰ value because of the confinement effect, for concrete in the column region, due to the presence of transversal rebars.
- Finally, a crushing strain equal to 8‰, corresponding to −2.24 mm of deformation for the link, is taken into account for collapse of the slab.

A similar modelling strategy is used to account for mechanism 2 in the component #5b, based on Eqs. (11) and (16) respectively, and the corresponding law can be seen in Fig. 12 (b). It can be observed – for the input parameters of the examined full-scale specimen – that mechanism 2 is less resistant (about ≈1.5 times) but especially remarkably less stiff (about ≈12 times) than mechanism 1. The resistance and stiffness terms

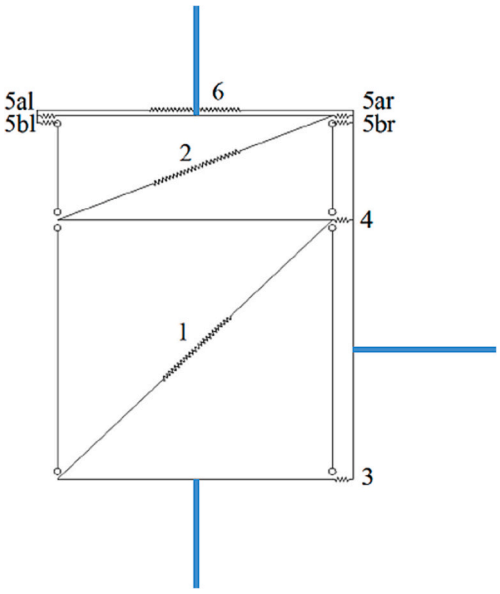

Fig. 11. Model #1 for exterior welded steel-concrete composite joint (Sap2000).

of link #6, which represents the longitudinal rebars in tension, are finally calculated based on Eqs. (19) and (23) respectively, see Fig. 12 (c). To note that a 0.28% slope is taken into account for hardening in component #6, based on the experimental results and material properties reported in [17]. Further, for the present simplified model, the maximum displacement is conventionally set in ±5 mm, which corresponds to a ± 2% strain and exceeds the ultimate strain of rebars in the full-scale specimen under cyclic loading [17]. The calculated constitutive laws for the other steel members can be found in Annex I.

Both a pushover and a cyclic analysis were carried out in Sap2000 with the mechanical model of Fig. 11. Typical results can be seen in Fig. 13, in terms of applied vertical force F and corresponding displacement d of the free cantilever end, where the present component-based modelling strategy is validated towards the available experimental evidences.

It is worth to note that, for the purpose of current modelling assessment, the numerical predictions discussed in [17] from the full 3D refined Abaqus model of Fig. 2 (a) are also presented in Fig. 13, and a rather good correlation can be observed among the collected plots. Remarkably, the computational efficiency of present modelling strategy is confirmed to represents a major advantage of the whole simulation approach. The number of elements and links for model #1 in Fig. 11, for example, is in fact limited to few units, while the 3D Abaqus assembly recalled in Fig. 13 is characterized by about ≈26,000 elements and 150,000 DOFs, with a consequent severe increase of the time of analysis.

From the experimental and numerical comparisons reported in Fig. 13, in particular, a more detailed analysis of results allows to see that the global stiffness of the specimen is correctly reproduced by model #1, with respect to experimental and 3D numerical values. This confirms that all the involved components for model #1 are efficiently characterized in mechanical terms, towards the real full-scale system. In

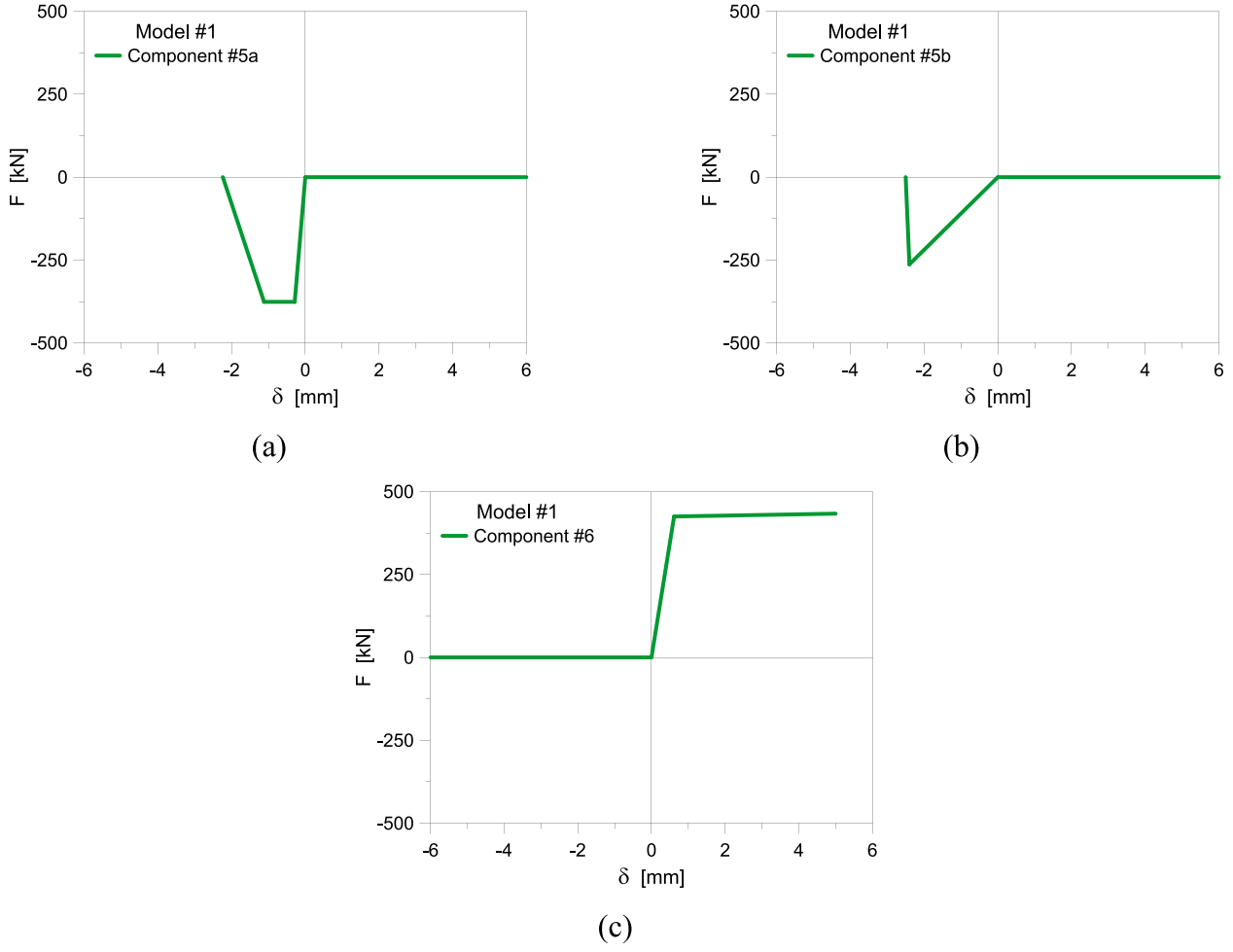

Fig. 12. Mechanical characterization of slab components: (a) #5a for mechanism 1 and (b) #5b for mechanism 2, with (c) steel rebars in tension (#6).

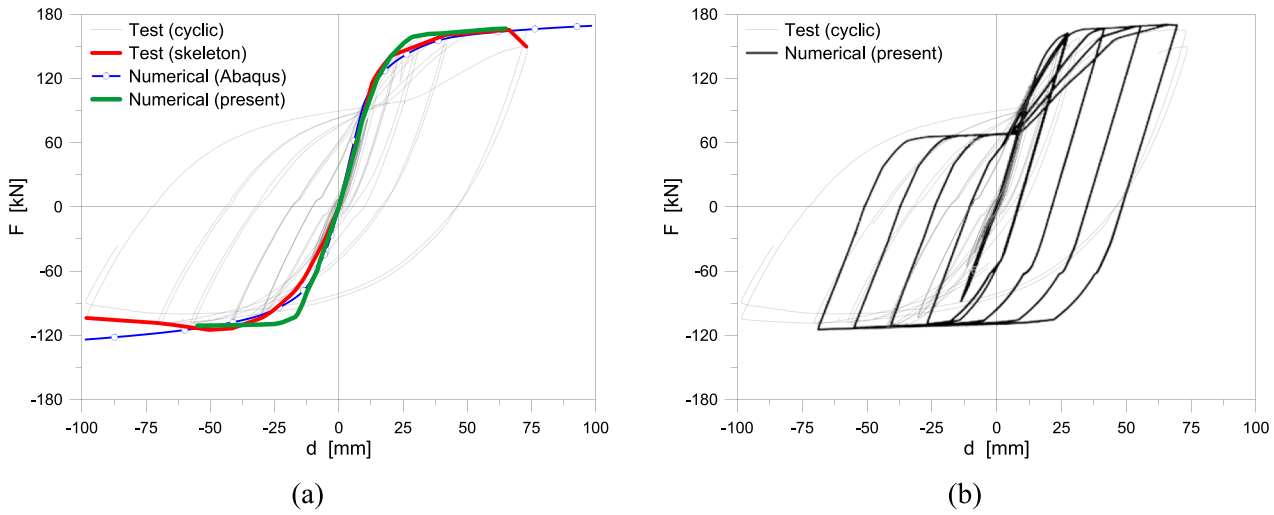

Fig. 13. Experimental validation of model #1 for exterior welded joint: (a) pushover and (b) cyclic numerical analysis (Sap2000). In evidence in figure (a), the numerical results from Abaqus model presented in [17].

terms of resistance, model #1 achieves a maximum force under positive bending moment which is equal to 167.8 kN (with 1.7% scatter compared to the experimental result). Under negative bending moment, the maximum recorded force is in the order of 110.35 kN for model #1, which slightly underestimates (4% scatter) the experimental result of 115 kN. In both cases, it is possible to conclude that most of the involved mechanisms are thus properly described by model #1 assembly and calibration, and the strategy can efficiently capture the global performance of steel-concrete composite systems.

In this regard, it is of interest to spend some further efforts for a more detailed analysis of components performance under cyclic loading (see Fig. 14). To this aim, the experimental and 3D numerical results discussed in [17] are used for further validation of present modelling strategy. The post-processing of model #1 outcomes shows in fact that:

- From Figs. 12 (a) and (b), it can be seen that mechanism 1 (#5a) is significantly stiffer than mechanism 2 (#5b). In this sense, see Fig. 14 (a), the response of the concrete slab is governed by mechanism 1, which is required to carry on the majority of the sustained load for the joint. It is of interest to note that the prevailing contribution of mechanism 1 was also confirmed by the detailed experimental and 3D numerical analysis discussed in [17] for the same full-scale specimen. Fig. 14 (b) shows in fact the distribution of compressive stresses in the slab at a vertical displacement $d = -40$ mm for the beam. This condition corresponds to the slab in tension schematized in Fig. 8, and reminds that the compressive stress distribution in the slab as for mechanism 1 of Fig. 8 (a) is characterized by the typical inclined struts.
- For the present model #1, it is assumed that concrete reacts only in compression and has null capacity in tension. Fig. 14 (c), in this regard, further confirms the critical role of mechanism 1 for the overall performance of the concrete slab, with crushing for the concrete in contact with the column and – in the tensile zone – the propagation of major cracks in the slab itself. This effect was highlighted in [17] in terms of experimental and 3D numerical failure mechanism for the slab in tension, where the premature propagation of major cracks was observed for relatively small imposed displacements. Certainly, model #1 is not able to capture such a detailed damage scenario for concrete in tension. However, the tensile failure mechanism evidenced in Fig. 14 (c) in terms of contour plot of DAMAGET parameter at $d = -10$ mm, confirms the present assumption of null load-bearing capacity for the concrete slab components #5a and #5b in tension (i.e., Figs. 12 (a) and (b)), and the tensile contribution of steel rebars only (Fig. 12 (c)).
- Under cyclic loading, finally, the column web suffers for yielding and partial plastic deformation only. This effect, which was experimentally observed in [17] for the full-scale specimen, is also confirmed in Fig. 14 (d) by the plastic response of component #1 in model #1. To note that component #1 yields at ±0.47 mm (Annex I) and even in cyclic conditions (with $d = \pm 65$ mm the maximum displacement of cantilever, see Fig. 13 (b)), the measured displacement for component #1 is quantified in about −0.88 mm (Fig. 14 (d)), which corresponds to limited post-yielding deformation, compared to its overall plastic capacity. Considering the length of link #1 and the measured force-displacement response in Fig. 14 (d), its mechanical performance can be used to roughly quantify a ≈ 0.15% plastic strain for the web panel. In this regard, it is of interest to remind that a similar response was confirmed by the full 3D model presented in [17] and herein proposed in Fig. 14 (e), for $d = 40$ mm. It can in fact be seen from the PEEQ contour plot that, even under large displacements, the peaks of plastic strain are mostly located in the beam flange rather than in the column web. Also, the corresponding PEEQ values in the web panel are measured in the order of ≈0.3–0.4% in the top corner and ≈0.1% in the bottom region, which means again a limited plastic deformation of the web panel, and in particular supports the above observations for component #1.

4.3. Model #2 – Exterior bolted joint

The second examined joint is similar to model #1, with the exception that the structural interaction of steel beam and column is given by a bolted joint with flange plate at the end of the beam, see Fig. 15. The specimen, in accordance with Section 4.2, was experimentally investigated in [24].

The presently assembled mechanical model #2, as shown in Fig. 16, includes up to 10 different link components. To note that links from #1 to #6 are defined and mechanically characterized in accordance with Section 4.2, and are thus not described further. The additional mechanical contributions for model #2, see also Annex II, are represented by:

- #7: column web, which works in series to the T-stub component;
- #8: T-stub component, on the side of column;
- #9: single bolt;
- #10a, #10b: T-stub components on the side of the beam.

According to Fig. 16, the column web contribution as in component #7 can be calculated like for #3 and #4, see Annex II. Of major interest

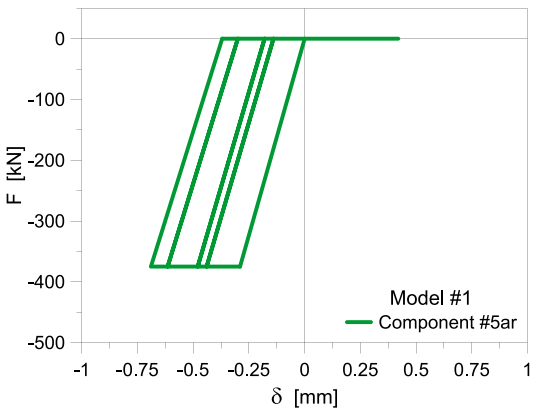

(a)

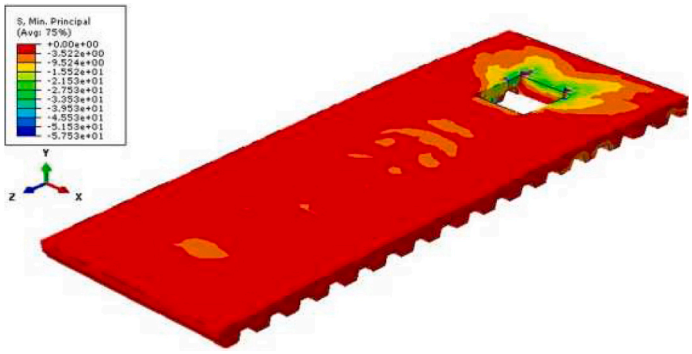

(b)

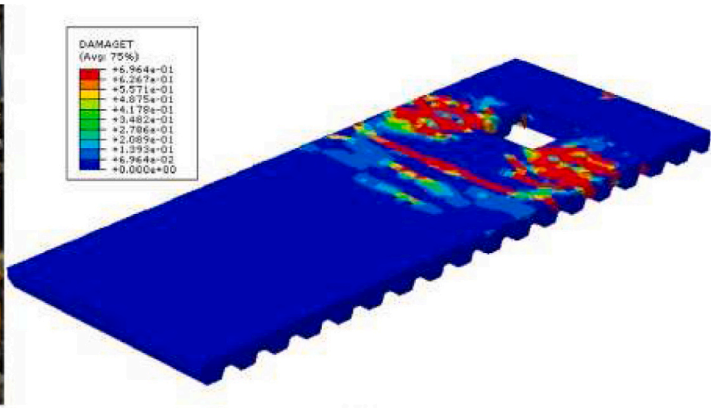

(c)

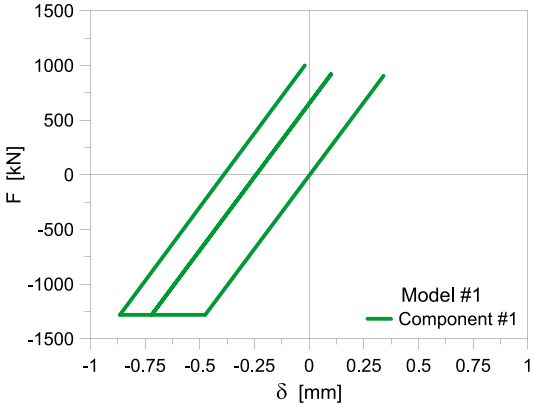

(d)

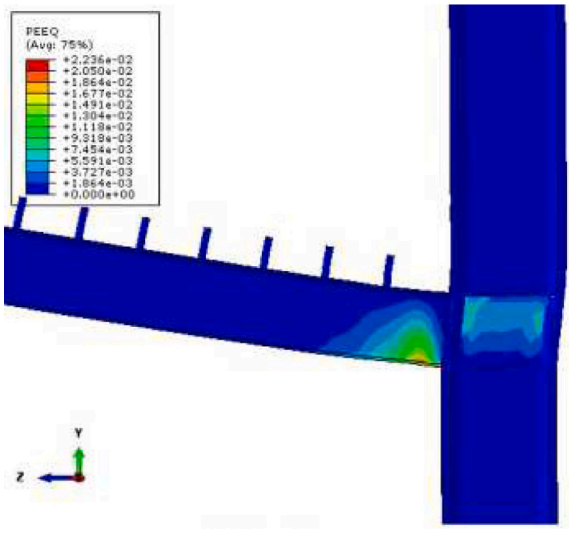

(e)

Fig. 14. Detail of cyclic performance in model #1 (Sap2000): (a) component #5ar, with (b) compressive stress distribution in the slab (legend in MPa, scale factor = 1); (c) tensile failure mechanism (DAMAGET) in the concrete slab (scale factor = 1); (d) component #1, with (e) equivalent plastic strain (PEEQ) in the column web panel (scale factor = 10). Figures (b), (c) and (e) reproduced from [17] with permission from Elsevier©, copyright license number 5619240622715, August 2023.

is indeed the contribution of components #8 and #10a, #10b.

They are in fact calibrated according to Annex I. In particular, for component #8 (T-stub on column side), an elastic-plastic behaviour in tension and a rigid behaviour in compression are taken into account (Fig. 17 (a)). The ultimate resistance is given by the weakest T-stub mechanism, while the yielding value coincides with 2/3 the ultimate one.

A symmetric elastic-plastic model is used for each bolt (component #9 in Annex I), with kinematic hysteretic response. Mechanical parameters for components #10a and #10b (T-stub on the side of beam) are finally characterized similarly to component #8, as it can be seen from Fig. 17 (b). As for component #8, the constitutive law is thus

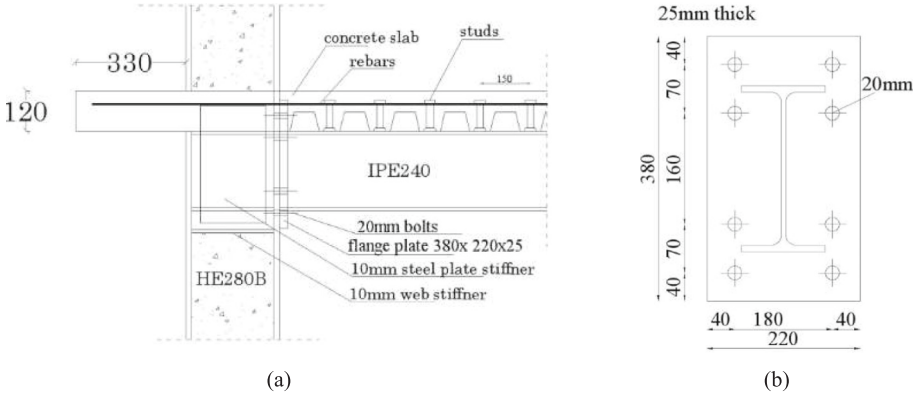

Fig. 15. Reference exterior bolted joint: (a) side view and (b) beam end flange (dimensions in mm). Reproduced from [24] with permission from Elsevier©, copyright license number 5619241091703, August 2023.

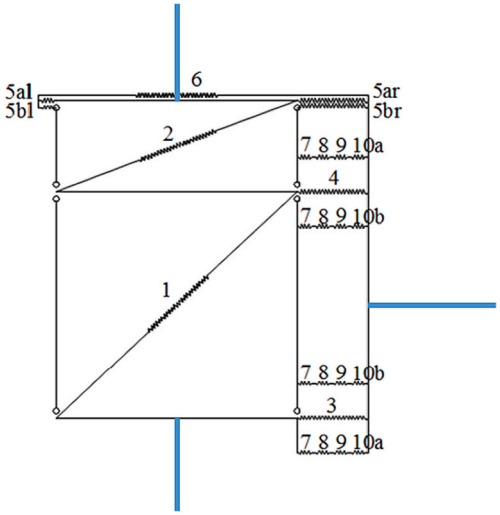

Fig. 16. Model #2 for exterior bolted steel-concrete composite joint (Sap2000).

elastic-plastic in tension and fully rigid in compression (see Annex I), with a Pivot hysteretic response.

From the analysis of results proposed in Fig. 18, it is possible to see that also model #2 well reproduces the monotonic and cyclic response of the bolted joint. In particular, the specimen stiffness is well captured under both positive and bending moments. In terms of resistance, the maximum force carried out by model #2 under positive bending moment is slightly scattered compared to the experiment, with 120 kN and 12% of underestimation (137 kN in the test). For the specimen under negative bending moment, the maximum force is again 120 kN for model #2 and 118 kN for the experiment (1.07% scatter), and this evidence still confirms a rather good potential of such a simplified modelling approach. It is important to note the drop of maximum positive force, which was mostly affected by crushing of concrete slab and null residual capacity.

As far as the cyclic response of individual components is explored, see Figs. 18-19, it can be noted that:

- The maximum force achieved by model #2 (Fig. 18) coincides with compressive failure of the concrete slab (Fig. 19 (a)). Afterwards, the slab itself is not anymore able to sustain additional loads. It is worth to note that this phenomenon, which is responsible of the major drop in the sustained maximum force, is well captured by model #2.
- In such a global mechanical response, a lower resisting contribution is numerically associated to mechanism 2, which is characterized – as already observed for model #1 – by reduced stiffness compared to mechanism 1 (Fig. 19 (b)).
- After collapse of the concrete slab, the reference experiment on the full-scale sample gave evidence of plastic failure in the bottom flange of the beam, with abrupt failure of the welding joint at the interface of beam end section and flange (Fig. 19 (c)). Such a behaviour is not captured by model #2, but it is in line with the original design of the

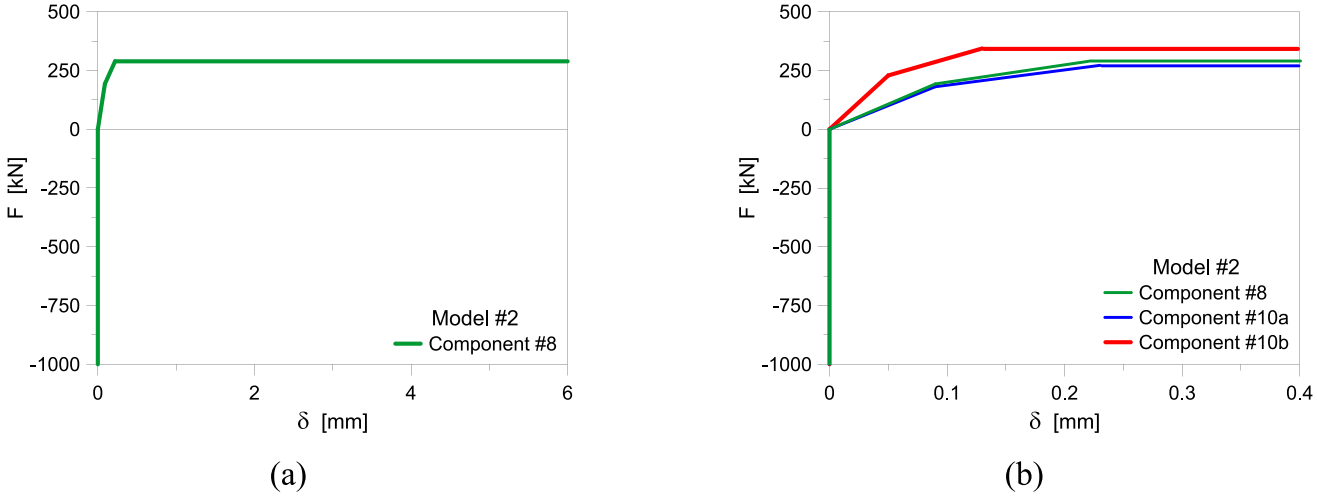

Fig. 17. Mechanical characterization of components: (a) #8 and (b) #10a, #10b.

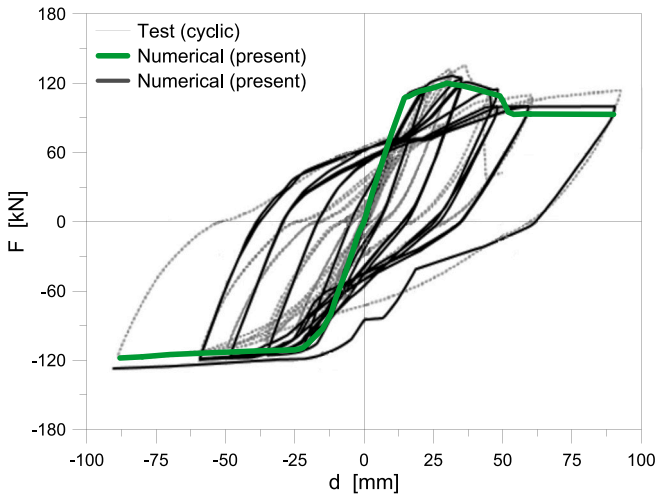

Fig. 18. Experimental validation of model #2 for bolted exterior joint: push-over and cyclic numerical analysis (Sap2000).

full-scale specimen (rigid joint with plastic hinge expected in the beam).

- According to the above observation, the overall performance of the specimen and of model #2 is associated to a minimum deformability contribution of the column web panel, while most of the overall deformation is assigned to the beam. Based on the local analysis of model #2 results, in this regard, it can be noted in Fig. 19 (d) that the column web panel remains elastic under cyclic loading and undertakes less than ±0.2 mm of total deformation, and this numerical finding is again in close correlation with the experimental observations reported in [24] for the full-scale specimen. Similarly, a major plastic response and deformability is numerically observed for the T-stub components on the side of column and beam, see Figs. 19 (e)-(f), which can remind – under the simplified assumptions of the present component-based modelling strategy – the stress peak concentration leading to the subsequent experimental collapse like in Fig. 19 (c).
- Finally, it is worth to note the different response of column web panel as in Fig. 19 (d), for model #2, rather than Fig. 14 (d), for model #1, where the fully elastic or plastic response respectively is emphasized for the component #1. In model #1, in particular, a displacement down to −0.88 mm was recorded for the joint analysis, which is more than ≈4 times larger the web panel deformation in model #2. The reason of such a different component response – which was also experimentally observed in [24], even with similar column web features – can be justified by the different stiffness contributions of all the involved joint components in models #1 and #2.

4.4. Model #3 – Interior bolted joint

The third examined joint, finally, is representative of the interior composite joint which was experimentally investigated in [11] and is schematized in Fig. 20 ("BR-X" specimen). The sample was assembled with a HEM260 column, IPE300 longitudinal beams and IPE270 transversal beams, to reproduce a typical interior joint belonging to a steel-concrete composite frame. The concrete slab was realized with total thickness of 120 mm and a profiled steel sheeting (Fig. 20 (b)), with longitudinal and transversal rebars schematized in Fig. 20 (a). The shear studs were placed as schematized in Fig. 20 (a). The displacement-controlled experiment was carried out by imposing a cyclic vertical load at the ends of IPE300 beams.

Similar to models #1 and #2, the herein assembled mechanical model #3 includes a set of links that are described as in Fig. 21.

Each component describes, more in detail, (#1) the column web panel in shear (below the stiffener steel plate); (#2) the column web panel in shear (above the stiffener); (#3, #4) the column web panel under compression or tension, due to the force which is transferred from the top and bottom beam flanges to the column; (#5a, #5b) mechanisms 1 and 2 for the concrete slab; (#6) longitudinal rebars in tension; (#7) the column web, which works in series to the T-stub component; (#8) the T-stub component, on the side of column; (#9) single bolt; (#10a, #10b) T-stub components on the side of the beam.

In addition to model #1 and #2, for the present configuration, the possible effect of mechanism 3 for the slab is also taken into account (#5c). To note that all the springs #5a, #5b, #5c are placed on the barycentric axis of the slab. All the components are calibrated as in Section 3, see Annex III.

In terms of numerical and experimental analysis of cyclic results, it can be seen from Fig. 22 that model #3 captures rather well the global mechanical performance of such a complex composite system. In terms of stiffness, for example, the numerical response is rather in good accordance with the experimental curve for the sample under negative bending moment, and still accurate for the sample under positive bending moment. The resistance is also well captured by model #3.

In terms of pushover analysis based on model #3, the effect and contribution of mechanism 3 from the slab in compression is also emphasized in Fig. 22, in terms of global force-displacement response of the joint. In this regard, it is worth to note that – from a numerical point of view – the mechanism 3 offers a negligible contribution to the resistance of the joint, and a null contribution in term of stiffness.

A more accurate analysis of experimental and numerical results in terms of component performance, as also summarized in Fig. 23, is thus helpful to confirm further the accuracy and potential of model #3.

At the time of the experiment discussed in [11], failure of the specimen was mostly affected by local buckling in the beam (Fig. 23 (a), after a displacement of 120 mm), subsequent few cracks in the slab in tension, as well as localized concrete crushing for the slab in contact with the column (Fig. 23 (b)). No clear evidence of resisting mechanisms in the slab was experimentally observed in [11], due to major yielding and plastic phenomena in the steel members. In particular, the bending moment observed in the transverse beams of specimen was found to remain near zero during the test, which means that the mechanism 3 was mostly not activated, and did not provide any resistance contribution to the slab.

While the present model #3 is not able to capture the local buckling phenomenon in the beam (and for this reason, the numerical analysis was carried out by limiting the imposed displacement to 120 mm only), a good qualitative correlation can be indeed observed for the overall performance assessment. Pushover results in Fig. 22, for example, still confirm the negligible effect of mechanism 3, and this is in line with the experiment described in [11]. Also, a major plastic contribution was numerically observed for the steel components, which is also in line with test results, see for example Figs. 23 (c)-(d)-(e).

5. Conclusions

The design and analysis of steel-concrete composite joints and frames under seismic loading, as known, are rather complex tasks which involve a multitude of geometrical and mechanical interacting parameters, within a variety of possible joint arrangements and configurations. In this sense, the availability of computationally efficient but still accurate numerical tools is of utmost importance for supporting design choices and assumptions.

In this paper, as a further elaboration and extension of earlier research efforts, a computationally efficient, non-linear component-based numerical modelling strategy was presented and experimentally validated in monotonic and cyclic conditions to predict the global and local response of steel-concrete composite joints, when subjected to seismic loads. The reference component-based numerical model, as shown, takes the form of a minimized number of links (for the active joint components) and composite frame sections (for the frame

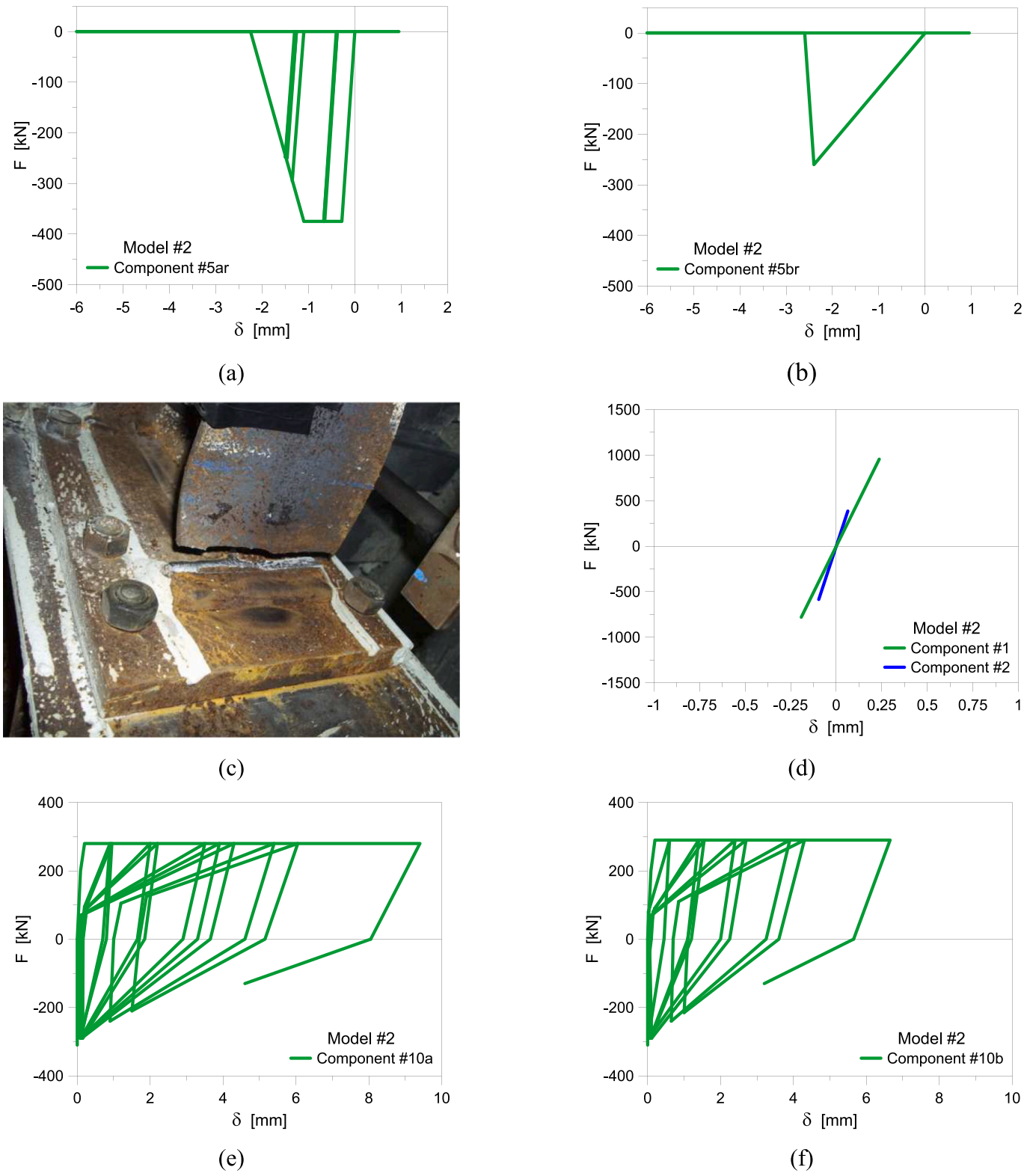

Fig. 19. Detail of cyclic performance for (a) components #5ar, (b) #5br (concrete slab); (c) detail of final collapse for the experimental specimen (reproduced from [24] with permission from Elsevier©, copyright license number 5619241091703, August 2023); components (d) #1 and #2 (column web in shear); components (e) #8 and (f) #10 (T-stub on the side of column or beam) respectively (Sap2000).

members) in which each element can be efficiently characterized in non-linear terms of resistance and stiffness coefficient. Non-linear stress-strain relationships with hysteretic models (Takeda for concrete, Pivot the T-stub components and kinematic for all the other steel members) are also considered to realistically characterize steel and concrete materials, while addressing the monotonic and cyclic performance of bolted and welded (both interior and exterior) composite joints. A major effort is given by the efficient description of slab mechanisms and interaction with the steel column, which requires special attention in such a geometrically simplified modelling procedure. In doing so, any

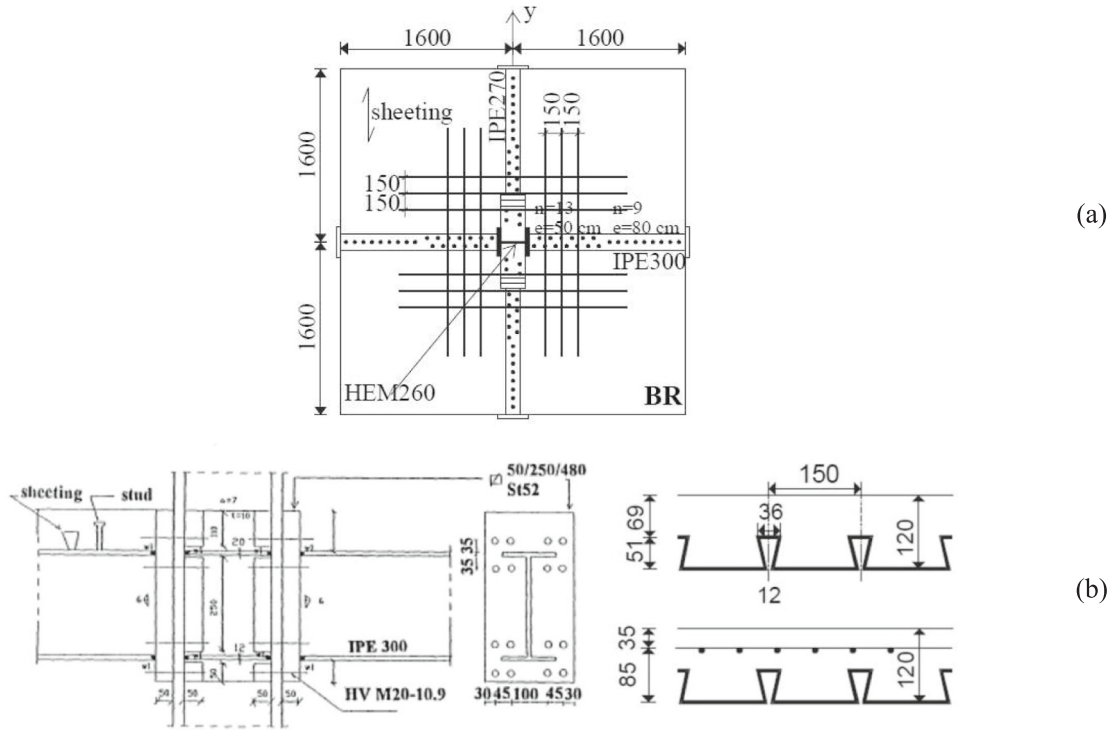

Fig. 20. Reference interior bolted joint: (a) top view; (b) joint detail with profiled steel sheeting (dimensions in mm).

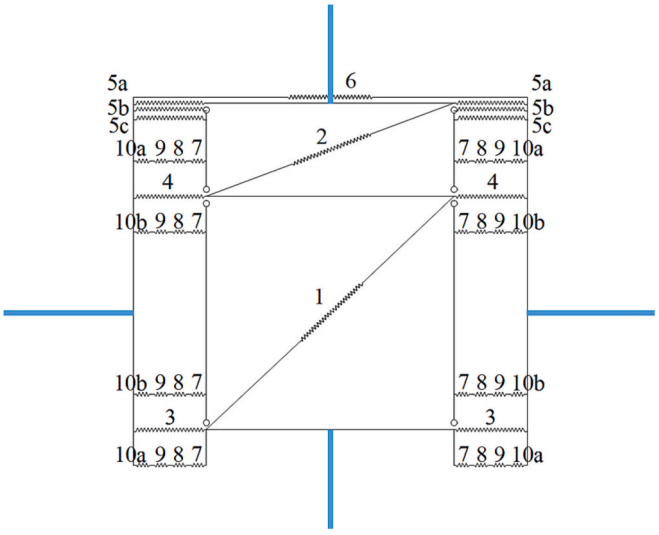

Fig. 21. Model #3 for interior bolted steel-concrete composite joint (Sap2000).

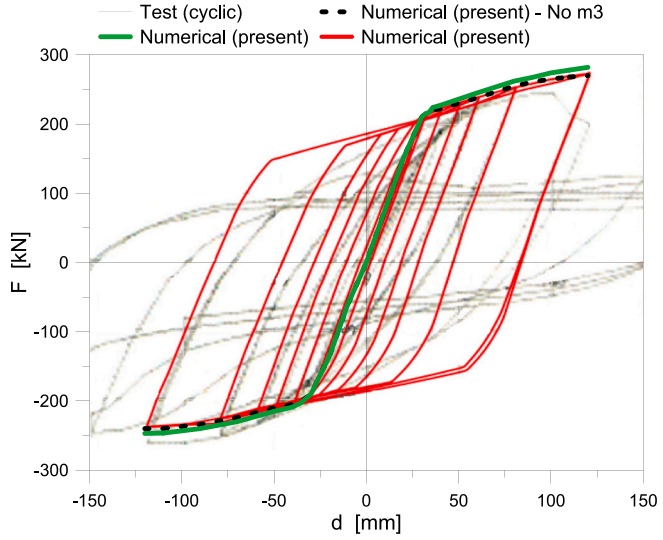

Fig. 22. Experimental validation of model #3 for interior bolted joint: push-over and cyclic numerical analysis (Sap2000).

king of tensile contribution for concrete is disregarded.

The validation of the unified numerical approach was carried out by comparisons of predictions with results of three selected full-scale specimens of literature, characterized by different configurations, mechanical properties and failure mechanisms. An exterior welded joint (model #1), an exterior bolted joint (model #2) and an interior bolted joint (model #3) were examined, under similar component-based modelling assumptions. As shown, even with a simplified modelling strategy, a rather close agreement was generally found between the present numerical predictions and the experimental mechanical response of the selected steel-concrete composite joints. Most importantly, the global force-displacement response was rather well captured for all of them. Also, the qualitative contribution of each component was rather well described, in most of cases, as also confirmed by the detailed analysis of component performances and a selection of past experimental or 3D numerical evidences. On the other side, it was also observed that the geometry simplification necessarily involves specific limits in terms of damage progress analysis, as it is for example for the progressive evolution of tensile cracks in the slab.

Finally, it is to note that the present strategy has remarkable benefits to support an optimized design process. From the discussion of comparative results, it was in fact shown that – depending on the nodal configuration – each component has a specific role and contributes to the overall mechanical response of the joint. In this sense, the contribution of steel members and concrete slab can be efficiently and uniformly taken into account (and optimized), regardless the typology or the detailing of a given joint. The most important feature is that the

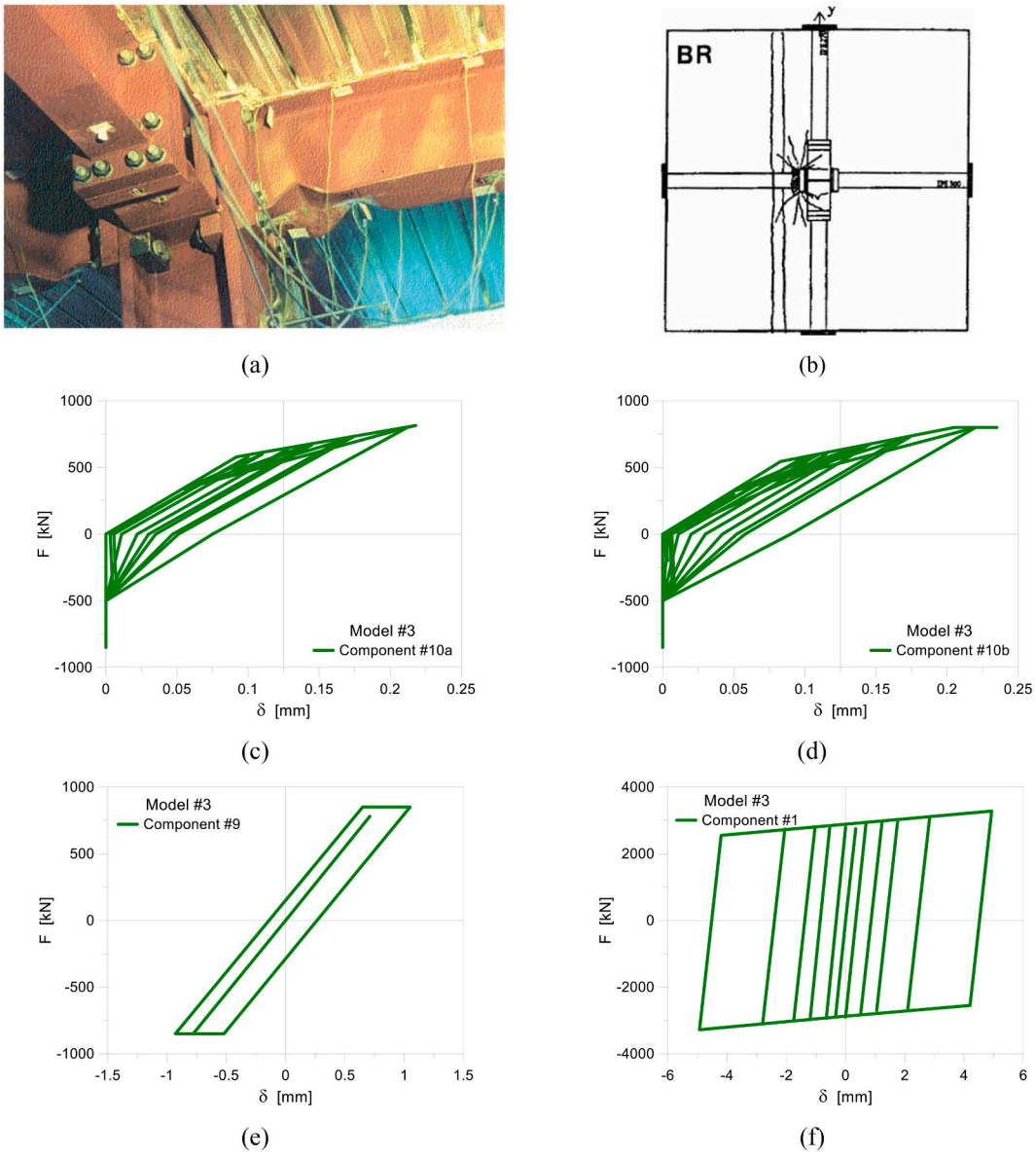

Fig. 23. Component performance of model #3: (a)-(b) experimental evidences (reproduced from [11]), with cyclic response of (c) T-stub on the side of column; (d) T-stub on the side of beam; (e) bolts and (f) column web panel (Sap2000).

possible resisting mechanisms in the concrete slab can be properly detected and optimized, based on design choices that (in line with Eurocode 8 provisions) will be necessarily voted to ensure a mostly dissipative behaviour with ductile failure in seismic conditions. As a further extension of present research efforts, new attempts will be devoted to the validation of the numerical strategy for the analysis of full steel-concrete composite frames, as well as to the refinement of cyclic degradation phenomena in the active components of the examined systems.

CRediT authorship contribution statement

Marco Fasan: Conceptualization, Methodology, Investigation, Data curation, Writing – original draft. **Chiara Bedon:** Methodology, Investigation, Data curation, Validation, Software, Writing – original draft. **Claudio Amadio:** Conceptualization, Methodology, Investigation. **Maria Rosaria Pecce:** Conceptualization, Methodology, Writing – original draft.

Declaration of Competing Interest

The authors declare there is no conflict of interest with the publication of present research study.

Data availability

Data will be made available on request.

Acknowledgements

DPC-RELUIS is gratefully acknowledged for funding the present research activity and for facilitating the scientific networking of the involved authors.

Appendix A. Appendix

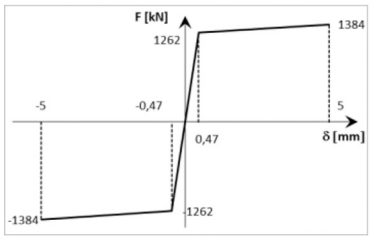

(a) Component #1

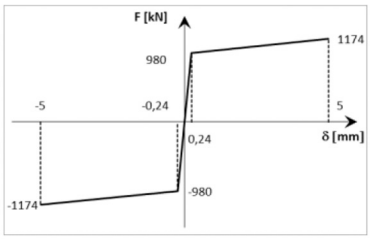

(b) Component #2

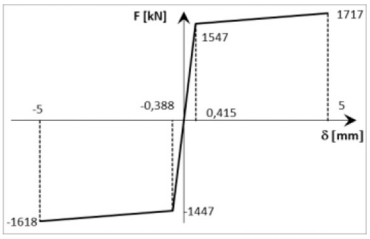

(c) Component #3 and #4

Annex I. Component characterization for model #1 (exterior welded joint).

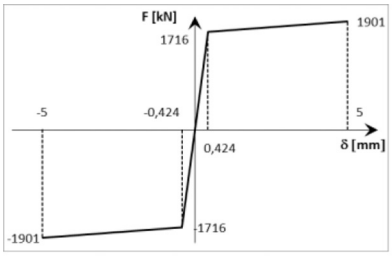

(a) Component #1

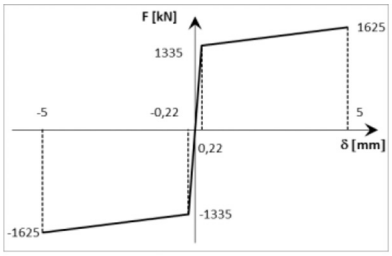

(b) Component #2

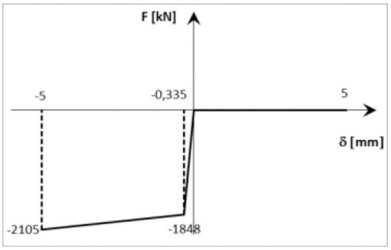

(c) Component #3 and #4

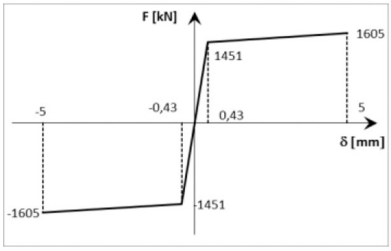

(d) Component #7

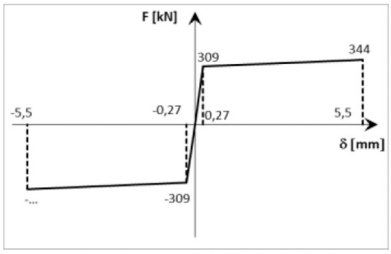

(e) Component #9

Annex II. Component characterization for model #2 (exterior bolted joint).

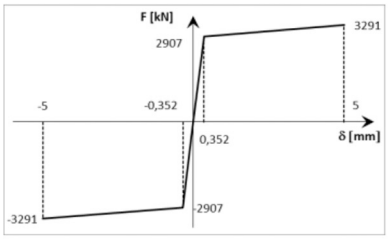

(a) Component #1

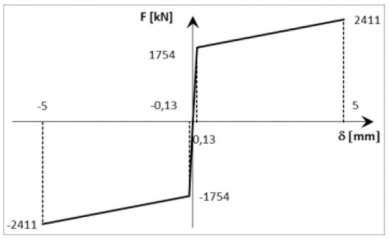

(b) Component #2

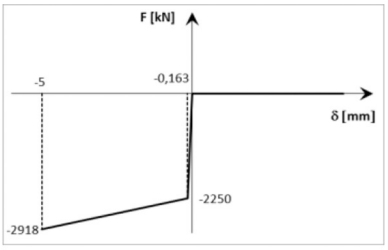

(c) Component #3

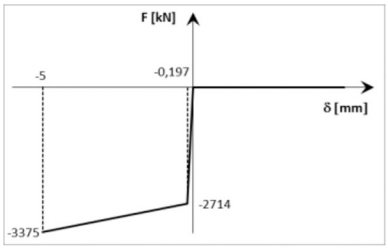

(d) Component #4

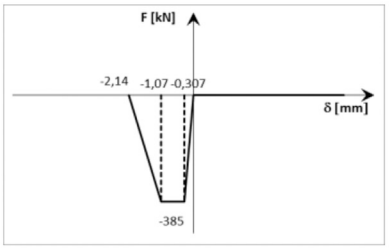

(e) Component #5a

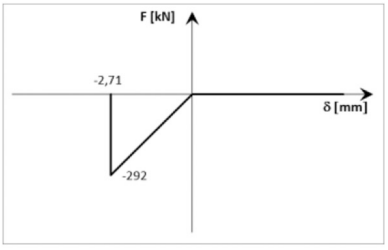

(f) Component #5b

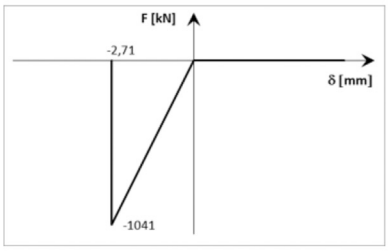

(g) Component #5c

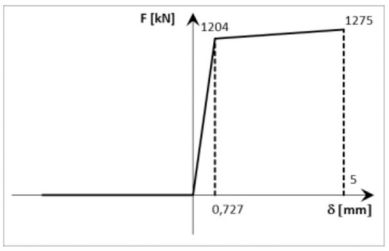

(h) Component #6

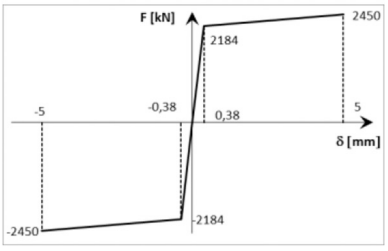

(i) Component #7a

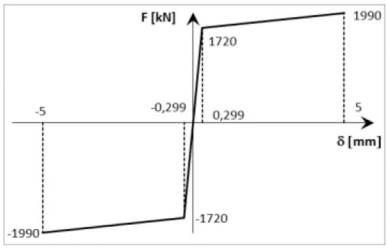

(j) Component #7b

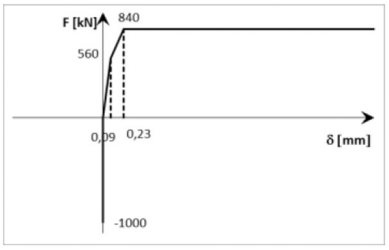

(l) Component #8

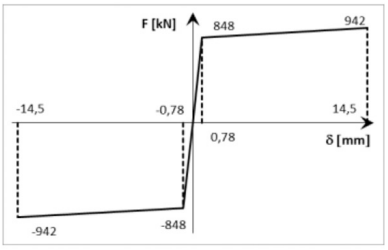

(m) Component #9

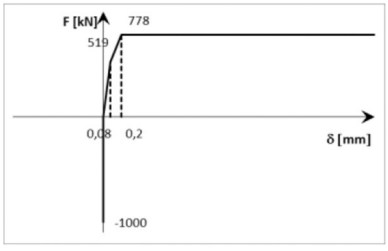

(n) Component #10a

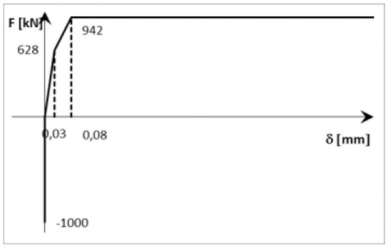

(o) Component #10b

Annex III. Component characterization for model #3 (interior bolted joint).

References

[1] A. Plumier, C. Doneux, J. Bouwkamp, G. Plumier, Slab design in connection zone of composite frames, in: Proceedings of the 11th European Conference on Earthquake Engineering, France, Paris, 1998.

[2] R.T. Leon, Analysis and design problems for PR composite frames subjected to seismic loads, Eng. Struct. 20 (4–6) (1998) 364–371.

[3] J. Aribert, A. Ciutina, D. Dubina, Seismic response of composite structures including actual behaviour of beam-to-column joints, in: Proceedings of the 5th International Conference on Composite Construction in Steel and Concrete V, 2006, pp. 708–717, https://doi.org/10.1061/40826(186)66.

[4] R. Liu, J. Wu, G. Yan, Q. Lai, H. Wang, Seismic performance of earthquake-resilient beam-to-column connection considering friction-slip mechanism, Journal of Building Engineering 75 (2023), 107055.

[5] Y.-X. Ma, K.H. Tan, Strength- and component-based model for steel beam to reinforced concrete column joint, Journal of Structural Engineering 149 (5) (2023), https://doi.org/10.1061/JSENDH.STENG-11446.

[6] I. Faridmehr, M. Nikoo, R. Pucinotti, C. Bedon, Application of component-based mechanical models and artificial intelligence to bolted beam-to-column connections, Appl. Sci. 11 (5) (2021) 2297.

[7] CEN, European Committee for Standardization, Eurocode 3: Design of Steel Structures - Part 1-8: Design of Joints, EN 1993-1-8, 2005.

[8] CEN, European Committee for Standardization, Eurocode 4: Design of Composite Steel and Concrete Structures - Part 1-1: General Rules and Rules for Buildings, EN 1994-1-1, 2005.

[9] CEN, European Committee for Standardization, Eurocode 8: Design of Structures for Earthquake Resistance - Part 1: General Rules, Seismic Actions and Rules for buildings, EN 1998–1, 2005.

[10] A. Plumier, European research and code developments on seismic design of composite steel concrete structures, in: Proceedings of the 12th World Conference on Earthquake Engineering (WCEE), New Zealand, Auckland, 2000.

[11] A. Plumier, C. Doneux, Seismic behaviour and design of composite steel concrete structures. European Commission – "Training and Mobility of Researchers" Programme – Innovative Concepts in Seismic Design "ICONS" Project. Technical report (198 pages) published by LNEC, Lisbon, Portugal, ISBN 972-49-1890-4, 2001. Available online at: https://orbi.uliege.be/bitstream/2268/61327/1/ICONS-Report.pdf.

[12] C. Amadio, M. Fasan, M.R. Pecce, G. Logorano, The guidelines for the design of steel-concrete composite moment resisting frames in seismic areas, in: Steel and Steel-Concrete Composite Structures in Seismic Area: advances in Research and Design. The Research Project RP3 of the ReLUIS-DPC 2014–2018 (Eds. Landolfo, Zandonini), 2018, pp. 211–244. ISBN 978–88–89972-74-8. Available online: https://arts.units.it/retrieve/e2913fdd-704d-f688-e053-3705fe0a67e0/chapter.pdf (last accessed on September 2023).

[13] Y.R. Liew, T.H. Teo, N.E. Shanmugam, Composite joints subject to reversal of loading – part 1: experimental study, J. Constr. Steel Res. 60 (2004) 221–246.

[14] A. Braconi, W. Salvatore, R. Tremblay, O.S. Bursi, Behaviour and modelling of partial-strength beam-to-column composite joints for seismic applications, Earthq. Eng. Struct. Dyn. 36 (2007) 142–161.

[15] G.A. Rassati, R.T. Leon, S. Noè, Component modeling of partially restrained composite joints under cyclic and dynamic loading, J. Struct. Eng. 130 (2) (2004) 343–351.

[16] I. Clemente, R.T. Leon, S. Noé, G.A. Rassati, Interpretation of the experimental behavior of two semi-rigid composite frames by means of a by-component mechanical model, in: Proceedings of the 5th International Conference on Composite Construction in Steel and Concrete V, 2006, pp. 674–685, https://doi.org/10.1061/40826(186)63.

[17] C. Amadio, C. Bedon, M. Fasan, M. Pecce, Refined numerical modelling for the structural assessment of steel-concrete composite beam-to-column joints under seismic loads, Eng. Struct. 138 (1) (2017) 394–409.

[18] C. Amadio, C. Bedon, M. Fasan, Numerical assessment of slab-interaction effects on the behaviour of steel-concrete composite joints, Journal of Constructional Steel Research 139 (2017) 397–410.

[19] R. Puhali, I. Smotlak, R. Zandonini, Semi-rigid composite action: experimental analysis and a suitable model, J. Constr. Steel Res. 15 (1990) 121–151.

[20] C. Amadio, F. Benussi, S. Noè, Modellazione di giunti semirigidi per la progettazione di telai composti, in: Proceedings of the 1st Italian Workshop on Composite Structures, Trento, Italy, 1993, pp. 195–212 (in Italian).

[21] E. Bayo, J. Cabrero, B. Gil, An effective component-based method to model semi-rigid connections for global analysis of steel and composite structures, Eng. Struct. 28 (2006) 97–108.

[22] C. Amadio, M. Bella, L. Macorini, A macro-model for beam-to-column connections in steel-concrete composite frames, in: Proceedings of ICSCS'10 – 4thInternational Conference on Steel & Composite Structures, 21–23 July 2010, Sydney, Australia, 2010, https://doi.org/10.3850/978-981-08-6218-3_CC-Fr002.

[23] U.E. Dorka, S. Amorntipsakul, Macro-elements for composite beam-column connections, in: Proceedings of the 6th International Conference on Composite Construction in Steel and Concrete VI, 2012, pp. 604–610, https://doi.org/10.1061/41142(396)49.

[24] M.R. Pecce, F. Rossi, The experimental behaviour and simple modelling of joints in composite MRFs, Eng. Struct. 105 (2015) 249–263.

[25] M. Fasan, C. Bedon, N. Troiano, C. Amadio, Improving the seismic capacity of steel–concrete composite frames with spiral-confined slabs, Adv. Struct. Eng. 25 (9) (2022) 1972–1987.

[26] C. Amadio, N. Akkad, M. Fasan, S. Noè, Modellazione in campo non lineare delle strutture composte intelaiate acciaio-calcestruzzo in zona sismica- Parte 1: Il giunto composto, Costruzioni metalliche 5 (2014) 36–42 (in Italian).

[27] M. Bella, Modellazione numerica di strutture sismoresistenti e analisi probabilistica di tipo Montecarlo, Università degli Studi di Trieste, Tesi di dottorato, 2009 (in Italian).

[28] J. Aribert, Influence of slip of the shear connection on composite joint, in: Proceedings of the 3rd International Workshop on Connections in Steel Structures, Italy, Trento, 1995.

[29] B. Gil, E. Bayo, An alternative design for internal and external semi-rigid composite joints. Part II: finite element modelling and analytical study, Eng. Struct. 30 (2007) 232–246.

[30] CSI Italia. Sap2000 – Integrated Software for Structural Analysis and Design, version 24.2.0; Computers and Structures Inc.: Berkeley, CA, USA.

[31] Simulia. ABAQUS Computer Software and Online Documentation, version 6.14; Dassault Systems: Johnston, RI, USA.